



An RB-Condensin II Complex Mediates Long-Range Chromosome Interactions and Influences Expression at Divergently Paired Genes

Aren E. Marshall,^{a,b} Charles A. Ishak,^{a,b*} Frederick A. Dick^{a,b,c,d}

^aLondon Regional Cancer Program, Lawson Health Research Institute, London, Ontario, Canada

^bDepartment of Biochemistry, Western University, London, Ontario, Canada

^cChildren's Health Research Institute, Lawson Health Research Institute, London, Ontario, Canada

^dDepartment of Pathology and Laboratory Medicine, Western University, London, Ontario, Canada

ABSTRACT Interphase chromosomes are organized into topologically associated domains in order to establish and maintain integrity of transcriptional programs that remain poorly understood. Here, we show that condensin II and TFIIC are recruited to bidirectionally transcribed promoters by a mechanism that is dependent on the retinoblastoma (RB) protein. Long-range chromosome contacts are disrupted by loss of condensin II loading, which leads to altered expression at bidirectional gene pairs. This study demonstrates that mammalian condensin II functions to organize long-range chromosome contacts and regulate transcription at specific genes. In addition, RB dependence of condensin II suggests that widespread misregulation of chromosome contacts and transcriptional alterations are a consequence of RB mutation.

KEYWORDS condensin II, TFIIC, epigenetics, chromosome architecture, gene expression, retinoblastoma protein, chromosome organization, regulation of gene expression

Genomes are more complex than their one-dimensional, linear DNA sequences. Three-dimensional organization of interphase chromosomes imparts regulatory information that contributes to development and disease. In particular, functions are arranged spatially in the nucleus such that transcription, replication, and other processes are compartmentalized in discrete locations (1). The organizational principles of interphase chromosomes and the molecular mechanisms by which architectural proteins contribute to chromosome organization are being revealed by chromosome conformation-based analysis (2). The convergence of signaling and environmental cues on transcription and chromatin remodeling machinery contributes to cell fate decisions (3). Not surprisingly, cell-type-specific chromosome territories have been observed and chromosomal rearrangements disrupting topologically associating domains (TADs) have been linked to cancer, further suggesting functional relevance of genome conformation (3, 4).

Higher-order chromosome organization is extensively supported by the structural maintenance of chromosomes (SMC) family of multisubunit protein complexes (5). In mammals, SMC family complexes include cohesin and condensins I and II (6). All contain two SMC subunits as well as unique non-SMC proteins. Specifically, cohesin contains SMC1 and SMC3, and condensins utilize SMC2 and SMC4. Condensins are further differentiated by their non-SMC subunits, with CAP-D3, CAP-G2, and CAP-H2 being unique to condensin II (6). All SMC-containing protein complexes form ring-like shapes that can entrap chromatin fibers to organize them into higher-order structures (5). The role of condensins in the compaction of chromosomes during prophase has been previously described in detail (7). Cohesins play a critical role in chromosome segregation in mitosis as well but have also

Citation Marshall AE, Ishak CA, Dick FA. 2020. An RB-condensin II complex mediates long-range chromosome interactions and influences expression at divergently paired genes. *Mol Cell Biol* 40:e00452-19. <https://doi.org/10.1128/MCB.00452-19>.

Copyright © 2020 American Society for Microbiology. All Rights Reserved.

Address correspondence to Frederick A. Dick, fdick@uwo.ca.

* Present address: Charles A. Ishak, Princess Margaret Cancer Centre, Toronto, Ontario, Canada.

Received 18 September 2019

Returned for modification 25 September 2019

Accepted 23 October 2019

Accepted manuscript posted online 4 November 2019

Published 3 January 2020

been determined to play an essential role in organizing the three-dimensional architecture of interphase chromosomes (8–12). Interestingly, studies show that some long-range chromosome contacts are preserved in the absence of cohesins, and condensin II cooccurs at some TAD boundaries (13, 14), suggesting it may also contribute to chromosome organization in some instances. However, in comparison to cohesin, the consequence of defective condensin II loading is relatively unexplored.

A number of lines of evidence suggest that abnormal chromosome topology in interphase is an important contributor to oncogenesis. Intergenic mutations and superenhancers have been shown to stimulate expression of distant oncogenes (15, 16). In addition, loss of chromosome topology due to chromosomal rearrangements has also been reported (17). Unfortunately, there are few examples to connect common cancer mutations with the systematic disruption of interphase chromosome topology (18). Therefore, it is unclear whether single gene mutations systematically alter chromosome topology on a routine basis. The retinoblastoma protein (RB) is typically known for its role in blocking cell cycle progression through E2F transcription; however, RB-deficient primary fibroblasts are known to possess relaxed chromatin in proliferating cells (19). Beyond null mutations, a partial loss-of-function murine *Rb1* mutation compromises condensin II recruitment to pericentromeric heterochromatin (20, 21). This mutation is a three-amino-acid substitution that disrupts the LXCXE binding site used by viral oncogenes called *Rb1^L* (22). Prior studies have shown that when RB-LXCXE interactions are disrupted, transcription from E2F-containing promoters is misregulated specifically under growth arrest conditions (22–24). However, during active proliferation, defective condensin II recruitment in *Rb1* mutant cells causes DNA replication-dependent damage at pericentromeric sequences (20), suggesting that RB may play a role in recruiting condensin II to interphase chromosomes for nonmitotic functions while cells proliferate.

To investigate condensin II regulation of chromosome structure in interphase cells, we utilized primary *Rb1^{L/L}* fibroblasts to disrupt condensin II recruitment. Using a combination of chromatin immunoprecipitation followed by high-throughput sequencing (ChIP-Seq), transcriptome sequencing (RNA-Seq), and chromosome conformation capture (3C) approaches, we demonstrate that RB recruits chromosome architectural protein complexes TFIIIC and condensin II to bidirectional promoters. Defective recruitment of condensin II diminished long-range chromosome contacts between bidirectional promoters and distant loci. In the absence of their recruitment, misexpression was observed at these gene pairs, suggesting that condensin II recruitment has effects on local transcription through alteration of chromosome topology. These experiments highlight transcriptional and architectural functions of an RB-condensin II complex that are obligatorily inactivated upon *RB1* loss in cancer.

RESULTS

Condensin II and TFIIIC occupy promoters in an RB-dependent manner. To investigate genome-wide localization of condensin II during interphase, we performed chromatin immunoprecipitation followed by high-throughput sequencing (ChIP-Seq) for CAP-D3, a subunit that is unique to condensin II, in asynchronously proliferating mouse embryonic fibroblasts (MEFs) which have a mitotic index of approximately 2% (22, 25). Regions of local enrichment were determined using model-based analysis for ChIP-Seq (MACS) (26). Using the *cis*-regulatory element annotation system (CEAS) (27), the distribution of CAP-D3 ChIP-Seq peaks within genomic features was determined and revealed that 40% of CAP-D3 peaks reside within 1 kb of a transcriptional start site (TSS) (Fig. 1A and B). We also carried out ChIP-Seq for CAP-D3 and CAP-H2 by using a combination of ethylene glycol bis(succinimidyl succinate) (EGS) and formaldehyde fixation to preserve protein-protein interactions that may recruit condensin II to chromatin and capture more interactions (Fig. 1C). This revealed more peaks by an order of magnitude and showed similar promoter occupancies (Fig. 1D and E), suggesting that condensin II commonly occupies promoters. Since CAP-H2 peaks intersect with CAP-D3 peaks at these promoters with more

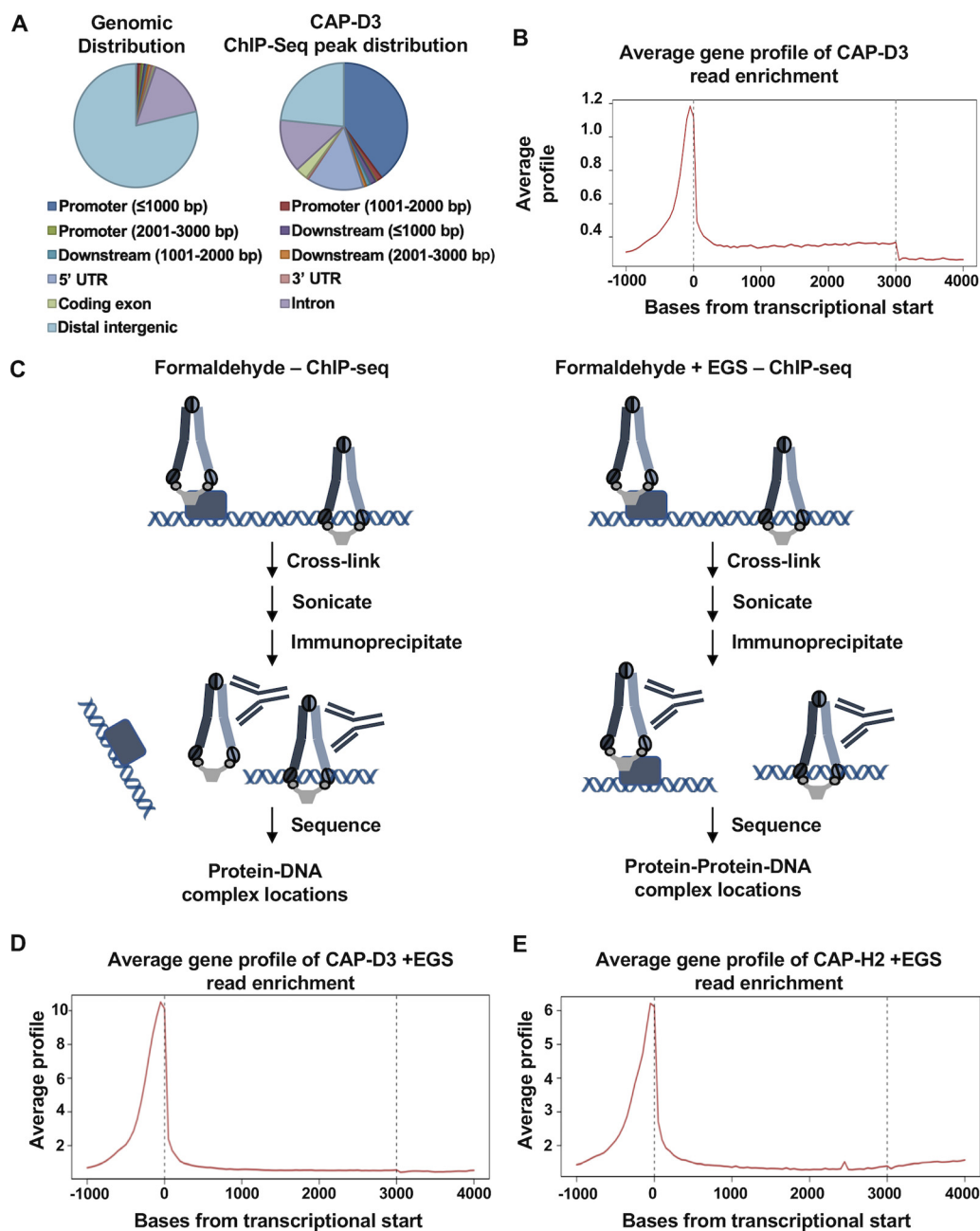


FIG 1 Condensin II localizes to proximal promoters. (A) Distribution of genomic features throughout the mouse genome and the distribution of *Rb1*^{+/+} CAP-D3 ChIP-Seq peaks within these genomic features. The category at the top of the pie chart (0°, or the 12 o'clock position) is "Promoter (≤ 1000 bp)," and the categories continue in order clockwise around the chart, with the legend being read from left the right. (B) Average distribution of *Rb1*^{+/+} CAP-D3 ChIP-Seq reads on a metagene, where gene length is scaled to 3,000 bp. (C) Schematic of captured ChIP fragments with formaldehyde versus formaldehyde and ethylene glycol bis(succinimidyl succinate) (EGS) fixation. Formaldehyde uses methylene bridges to cross-link and is primarily a protein-DNA cross-linker, whereas EGS is a protein-protein cross-linker, using *N*-hydroxysuccinimide (NHS) esters to yield stable amide bonds. Since condensin II may not directly bind to DNA at many locations with which it interacts, EGS/formaldehyde dual cross-linking was used to have a more in-depth look at chromatin contacts. (D) Average distribution of EGS- and formaldehyde-fixed CAP-D3 ChIP-Seq reads 1,000 bp upstream and 1,000 bp downstream of genes, where each gene length is scaled to 3,000 bp. (E) Average distribution of EGS- and formaldehyde-fixed CAP-H2 ChIP-Seq reads on a metagene, where gene length is scaled to 3,000 bp.

than 70% frequency, we conclude that these represent condensin II complexes and not free subunits.

Since RB recruits condensin II to pericentromeric heterochromatin (20), we compared CAP-D3 occupancy locations between wild-type and *Rb1*^{L/L} murine fibroblasts to

learn where RB-condensin II localizes in interphase nuclei. This *Rb1* mutant carries a missense allele designed to disrupt interactions with viral oncogenes such as the human papillomavirus (HPV) E7 gene, while preserving interactions with E2F transcription factors (22). Condensin II recruitment to pericentromeric heterochromatin is reduced in *Rb1^{L/L}* cells (20), but chromatin loading of cohesin and condensin I is normal (28). In addition, cooccupancy analysis by sequential chromatin immunoprecipitation (ChIP re-ChIP) for RB with both CAP-D3 and CAP-H2 has demonstrated that they form a complex (21). Through immunoprecipitation of RB followed by Western blotting for components of condensin II, CAP-D3, and SMC2, we reconfirmed previously published results demonstrating that RB interacts with condensin II in the chromatin fraction of wild-type MEFs but the *Rb1^L* mutation eliminates this (Fig. 2A) (28). Accordingly, through ChIP-Seq, approximately two-thirds of all CAP-D3 peaks found in wild-type MEFs were lost in the *Rb1^{L/L}* mutant. To examine RB dependency of CAP-D3 localization at promoters, CAP-D3 and input ChIP-Seq reads from *Rb1^{+/+}* and *Rb1^{L/L}* MEFs were normalized to $1 \times$ genomic coverage using reads per genomic content (RPGC), and the input signal was then subtracted from the ChIP signal. These normalized CAP-D3 ChIP-Seq signals were compared between the two genotypes at 1,271 promoters that were the most enriched for CAP-D3 (Fig. 2B). At these promoter locations in *Rb1^{L/L}* cells, CAP-D3 peaks are completely lost 30% of the time or are shifted or diminished at other locations, indicating that condensin II binding is influenced by the *Rb1^{L/L}* genotype.

Condensin recruitment in *Saccharomyces cerevisiae* is dependent on TFIIC (29), and condensin II and TFIIC colocalize on chromosomes in mammalian cells (13). To reconcile roles for RB and TFIIC in condensin II recruitment, we carried out ChIP-Seq for the TFIIC 220-kDa subunit in *Rb1^{+/+}* and *Rb1^{L/L}* MEFs. These data revealed that TFIIC is abundant just 3' of the TSS of promoter regions containing CAP-D3 peaks (Fig. 2C and D), and genome wide, a similar pattern of TFIIC binding at TSS is observed (Fig. 2E). Interestingly, TFIIC read buildups surrounding the TSS of promoter regions containing CAP-D3 peaks are reduced in *Rb1^{L/L}* MEFs (Fig. 2C and D). Using MACS, duplicate ChIP-Seq experiments were analyzed and revealed that 67% of the promoter views in Fig. 2C contain TFIIC peaks in *Rb1^{+/+}* cells. When TFIIC occupancy immediately 3' of the promoter end location is examined, only 42% of these peaks are maintained in *Rb1^{L/L}* cells, whereas other TFIIC peaks 5' of proximal promoters are relatively unaffected by the *Rb1^L* mutation. This indicates that recruitment of TFIIC and condensin II is RB dependent, specifically at these TSS locations.

To further examine the dependency of condensin II and TFIIC binding on RB at promoter regions and to quantify changes in binding, the *Timm13* promoter/*Lmn2* origin of replication was investigated, as this is an example of a CAP-D3 peak location that was retained, but reads are diminished in ChIP-Seq from *Rb1^{L/L}* cells (Fig. 2F). Quantitative assessment of CAP-D3 binding at *Timm13/Lmn2* by ChIP-qPCR reveals that CAP-D3 binding is significantly enriched over the control IgG background only in *Rb1^{+/+}* MEFs and that TFIIC also shows RB-dependent enrichment at this locus (Fig. 2G to I). This indicates that condensin II and TFIIC are reliant on RB for recruitment to specific chromosomal loci.

RB-condensin II complexes regulate expression at bidirectional promoters. The gene promoters occupied by condensin II were subject to functional annotation clustering using the Database for Annotation, Visualization and Integrated Discovery (DAVID) (30). This analysis demonstrates diverse functional categories, such as DNA damage repair, cell division, transcription, and translation (Fig. 3A). Interestingly, querying these promoter locations returned substantially more genes, implying that many condensin II binding sites occur in bidirectional promoters. RB-condensin II-occupied locations are enriched for bidirectional promoters in comparison to their frequency of promoter regions within the genome (Fig. 3B), and this exceeds the proportion of bidirectional promoters expected by chance (Fig. 3C).

RNA-Seq and expression microarrays were then used to investigate whether *Rb1^{L/L}* MEFs display changes in expression of these genes (Fig. 3D). Analysis of expression of

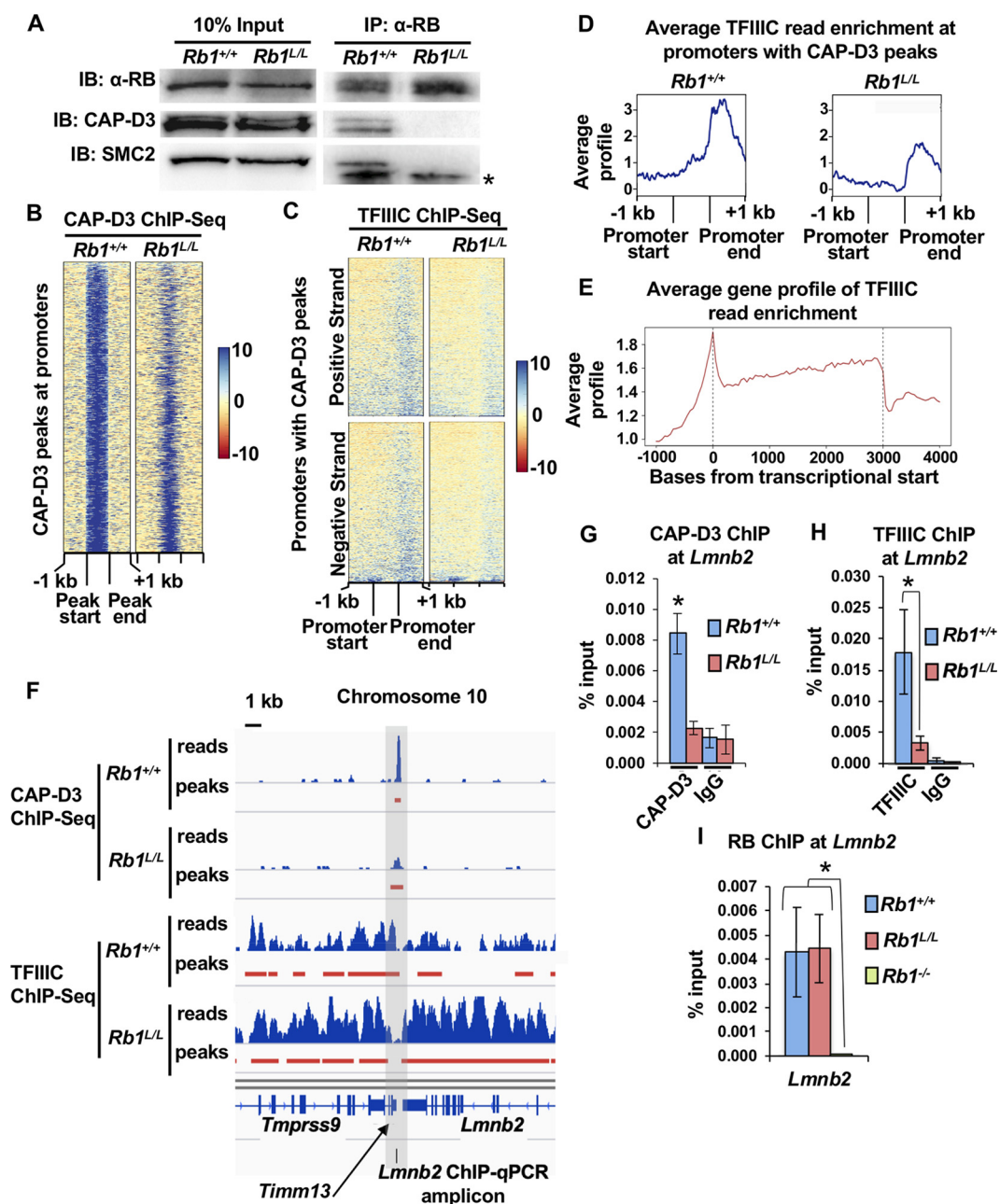
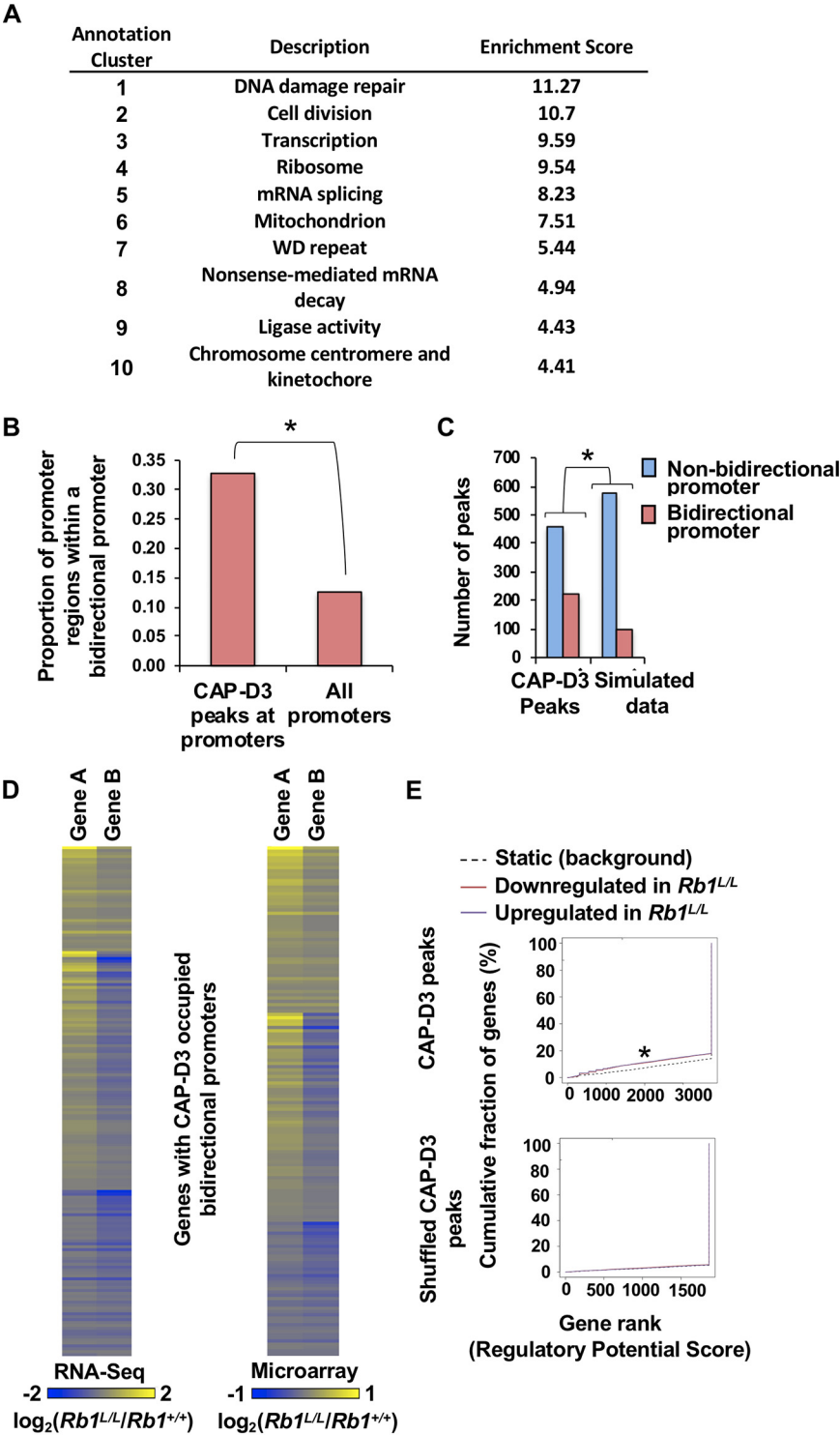


FIG 2 RB recruits TFIIC and condensin II to proximal promoters. (A) Extracts were prepared from asynchronously cycling *Rb1*^{+/+} and *Rb1*^{L/L} MEFs, and the chromatin fractions from these cells were subjected to immunoprecipitation (IP) with an anti-RB antibody. The relative amounts of RB, CAP-D3, and SMC2 that precipitated with wild-type and mutant RB were detected by Western blotting. The lower band visible from the IP fractions of both genotypes in the SMC2 immunoblot image represents background, as indicated by an asterisk. (B) Heat maps of CAP-D3 ChIP-Seq read abundance at 1,271 promoters that contain a CAP-D3 peak in *Rb1*^{+/+} cells. CAP-D3 and input ChIP-Seq reads from *Rb1*^{+/+} and *Rb1*^{L/L} MEFs were normalized to 1× genomic coverage using RPGC, followed by the subtraction of input signal from the ChIP signal. (C) Heat maps of TFIIC ChIP-Seq read abundances in *Rb1*^{+/+} and *Rb1*^{L/L} MEFs at the same genome locations as described for panel B and normalized using the same procedure. (D) Average distribution of *Rb1*^{+/+} and *Rb1*^{L/L} TFIIC ChIP-Seq reads from the positive-strand heat maps in panel C. (E) Average distribution of *Rb1*^{+/+} TFIIC ChIP-Seq reads on a metagene, where gene length is scaled to 3,000 bp. (F) ChIP-Seq tracks for CAP-D3 and TFIIC from *Rb1*^{+/+} and *Rb1*^{L/L} MEFs at the *Timp13* promoter/*Lmn2* origin. Read buildup scale is 25. (G) ChIP-qPCR for CAP-D3 and IgG controls at the *Lmn2* origin of replication (*n* = 4). (H) ChIP-qPCR for TFIIC and IgG controls at the *Lmn2* origin of replication (*n* = 4). (I) ChIP-qPCR for RB at the *Lmn2* origin of replication (*n* = 3). All error bars are ±1 standard error of the mean (SEM); *, *P* < 0.05, *t* test.



(Continued on next page)

genes on either side of bidirectional promoters bound by CAP-D3 in *Rb1*^{+/+} MEFs demonstrates that at many of these locations, changes in expression occur at these gene pairs in *Rb1*^{L/L} cells. At these locations, there is not a single directionality of these gene expression changes; both genes can be upregulated, both can be downregulated, and one gene can be upregulated while the other gene is downregulated. Local contributions to the differential gene expression in *Rb1*^{L/L} cells was further investigated using Binding and Expressing Target Analysis (BETA) (31), to relate CAP-D3 peak locations with RNA-Seq expression changes of nearby genes, taking into account CTCF binding sites and its regulatory boundaries (Fig. 3E). Cumulative gene percentages that are higher than background suggests that repressive and activating influences occur at neighboring genes. Position-shuffled CAP-D3 peaks do not correlate with transcript changes in *Rb1*^{L/L} MEFs compared to *Rb1*^{+/+} MEFs, further validating this correlation and suggesting a functional connection between condensin II occupancy and nearby gene expression.

There are a number of potential explanations for gene expression changes at bidirectional promoters in *Rb1*^{L/L} cells. First, the cell cycle category identified by DAVID suggests that these patterns may simply reflect misregulation of classical RB-E2F transcripts. However, analysis of 52 established RB-E2F transcriptional targets reveals only partial occupancy by CAP-D3 (Fig. 4A), and in asynchronously proliferating and serum-starved *Rb1*^{L/L} cells, these genes are significantly less altered in transcript abundance than the previously characterized *Rb1*^G mutant that is defective for E2F binding (32) (Fig. 4B and C). In contrast, gene expression changes at the CAP-D3-occupied bidirectional promoters in proliferating *Rb1*^{L/L} cells are largely absent from serum-starved *Rb1*^{G/G} and *Rb1*^{L/L} cells. This is evident in heat maps depicting changes at individual bidirectional promoters and in absolute gene expression values (Fig. 4D and E). These analyses demonstrate that there is a level of specificity to the gene expression changes seen in different *Rb1* mutants. This emphasizes that misregulation of these bidirectional promoters when the *Rb1*^L mutant is unable to recruit condensin II is not a byproduct of altered RB-E2F transcriptional control.

Another possible explanation for gene expression changes in *Rb1*^{L/L} cells at bidirectional promoters is that they may be the consequence of chronic DNA damage previously reported in these cells (20). Since DNA damage repair is the most enriched functional category in these bidirectional promoters, we investigated their expression changes in *Rb1*^{L/L} fibroblasts. This revealed that genes involved in DNA damage repair were both upregulated (11 genes) and downregulated (15 genes). Since these data fail to reveal a consistent trend, they further suggest that gene expression changes are not a response to DNA damage.

To gain further insight into condensin II's potential role, and to further rule out previously described functions for RB as an explanation for our observations, we investigated the chromatin state of these promoters. In wild-type MEFs, there is extensive simultaneous occupancy of these promoters with Pol2 and H3K4me3, which suggests that there is active transcription (33) (Fig. 4F), and there was 98% peak overlap between these modifications and CAP-D3-containing promoters. H3K27ac, a mark of active enhancers and promoters, is also highly abundant at these promoters, with 85% overlap (33–35). Conversely, repressive chromatin marks such as H3K27me3 and H3K9me3 were almost completely excluded from these promoters (Fig. 4F), with 2% and 1% peak occupancies, respectively. The most obvious conclusion from this work is that RB-condensin II complexes are localized to active promoters. Importantly, this pattern of histone modifications is highly divergent from known regulatory roles for RB in gene silencing that are characterized by the establishment of H3K9me3 in senes-

FIG 3 Legend (Continued)

in the middle, and those that have a decrease in expression of both genes are on the bottom. (E) Binding and Expressing Target Analysis (BETA) was used to determine that CAP-D3 peaks correlate with local changes of RNA-Seq gene expression between *Rb1*^{L/L} and *Rb1*^{+/+} MEFs, taking into account CTCF binding sites. *, *P* < 0.05. Computationally "shuffled" peaks are not correlated with transcriptional changes.

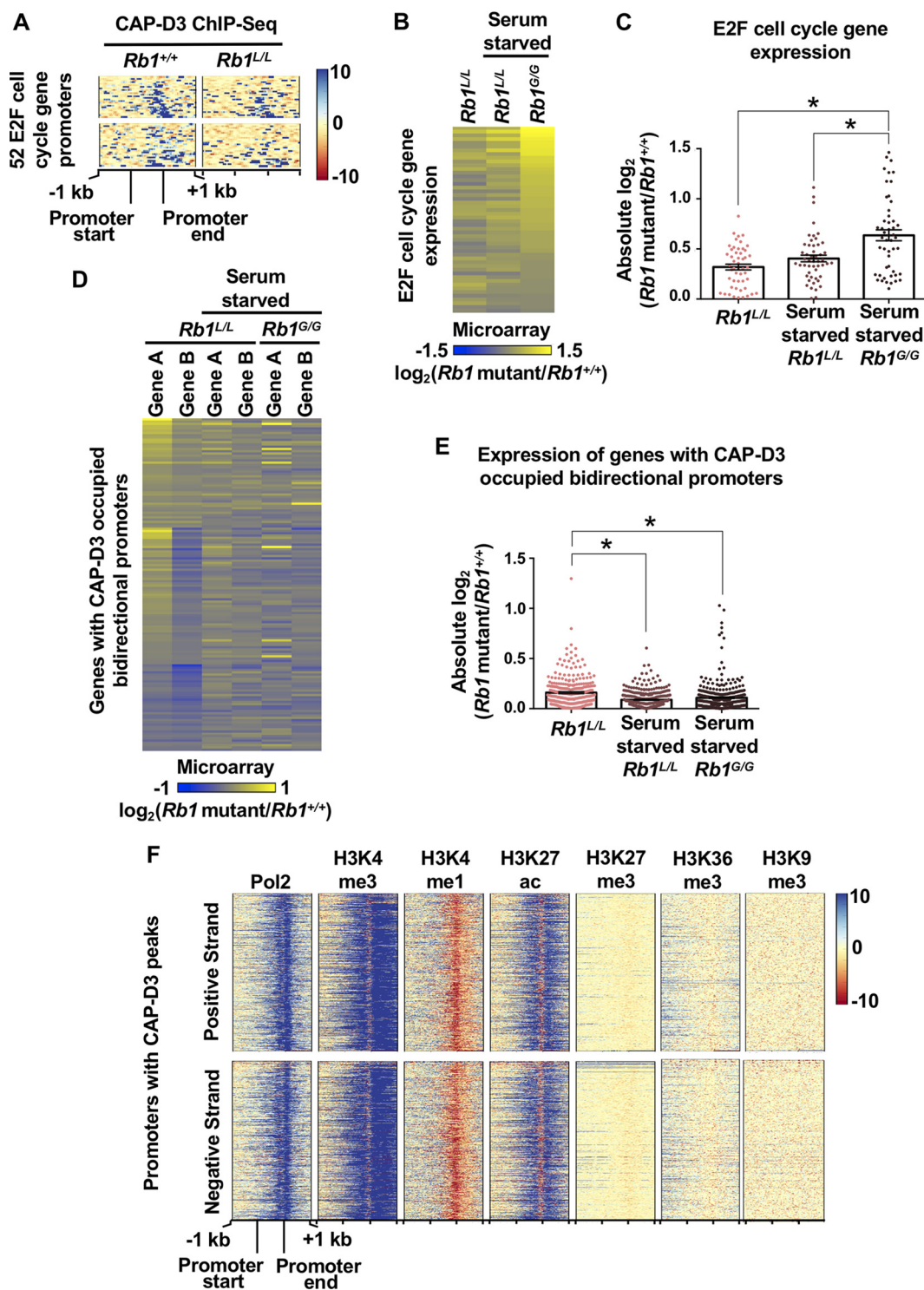


FIG 4 Condensin II target genes are distinct from classic E2F target genes. (A) Heat maps of CAP-D3 ChIP-Seq read abundance relative to input controls in *Rb1*^{+/+} and *Rb1*^{L/L} MEFs at 1-kb proximal-promoter regions of 52 RB-regulated E2F cell cycle target genes. Heat maps are divided into those promoters on the forward strand (top) and those on the reverse strand (bottom). (B) Expression microarray data were used to compare abundances of these 52 transcripts between proliferating *Rb1*^{L/L} MEFs and serum-starved *Rb1*^{L/L} and *Rb1*^{G/G} cells, all compared to the wild type. The average expression for three *Rb1* mutant MEF preparations relative to three wild-type preparations is shown. (C) The absolute values of the expression changes in the *Rb1* mutant MEFs compared to *Rb1*^{+/+} MEFs from panel B were compared. The RB-regulated E2F cell cycle target gene transcripts were significantly more misexpressed in *Rb1*^{G/G} MEFs than in *Rb1*^{L/L} MEFs grown under either condition. (D) Expression microarray data are shown comparing abundances of transcripts at bidirectional promoters occupied by CAP-D3 between proliferating *Rb1*^{L/L} MEFs and serum-starved *Rb1*^{L/L} and *Rb1*^{G/G} MEFs, all normalized to wild-type MEFs. Each row represents a bidirectional promoter occupied by CAP-D3, and gene A and gene B arbitrarily refer to gene pairs at a given bidirectional promoter. (Continued on next page)

cence (36), H3K27me3 in terminal differentiation during development (37), and deacetylation of histones in quiescence (36). This further emphasizes that RB recruitment of condensin II to these promoters represents a functional paradigm that is different from previous functions. An intriguing result is the apparent asymmetric upregulation of one gene at some condensin II-occupied bidirectional promoters in *Rb1^{L/L}* cells (Fig. 3D). In this scenario, condensin II may function to create different transcriptional environments between closely spaced promoters. We selected two bidirectional promoters for more detailed analysis to understand misregulation at one of these gene pairs.

RB-condensin II complexes mediate long-range chromosome interactions. We focused our mechanistic characterization on the *Usp5/Cdca3* and *Pxmp2/Pole* bidirectional promoters because quantitative reverse transcription-PCR (RT-qPCR) confirmed that there was misexpression of one of the gene pairs in *Rb1^{L/L}* and *Rb1^{-/-}* cells (Fig. 5A). In addition, ChIP experiments demonstrate that RB occupies these promoters and that condensin II subunits and TFIIC exhibit RB-dependent enrichment at these loci (Fig. 5B to E). When the *Rb1^L*-encoded protein is present, but unable to assemble this complex, expression of one gene in each pair is elevated, implicating TFIIC and condensin II in this regulatory event.

Loss of condensin II function affects progression through mitosis (38), and *Rb1^{L/L}* MEFs similarly display misshapen chromosomes, mitotic delay, and aneuploidy in daughter cells (22, 28). Studies of condensin mutants in fission yeast suggest that gene misexpression may be a consequence of mitotic errors and aneuploidy (39). Therefore, to create aneuploidy in *Rb1^{+/+}* MEF cells and to increase G₂/M phase levels to be similar to those in *Rb1^{L/L}* fibroblasts, nocodazole was used to inhibit mitotic progression (Fig. 6A and B). This induced mitotic errors and delayed progression but did not cause expression changes at the *Usp5/Cdca3* and *Pxmp2/Pole* bidirectional promoters (Fig. 6C). This suggests that indirect effects on transcription from defective condensin II function in mitosis in *Rb1^{L/L}* cells is unlikely to explain misregulation at these bidirectional promoters.

Genome views of *Usp5/Cdca3* and *Pxmp2/Pole* reveal numerous condensin II subunit peaks distributed across surrounding regions (Fig. 7A and D). We explored whether this distribution indicated that condensin II organizes local intrachromosomal loops between these locations to influence gene expression at these bidirectional promoters. We performed four chromosome conformation capture (3C)-qPCR experiments on wild-type and *Rb1^{L/L}* MEF pairs using *Usp5/Cdca3* and *Pxmp2/Pole* as the reference points (Fig. 7B and E). These experiments revealed sites of local interaction; however, loops appeared in locations that were unrelated to condensin II peaks (Fig. 7C, +60 kb from *Cdca3* bait). Furthermore, no local interactions were gained or lost between genotypes within these regions (Fig. 7C and F).

To broaden our search for condensin II-dependent chromosome interactions, we carried out 16 circularized chromosome conformation capture (4C)-Seq experiments using the same promoters as bait (four independent experiments for each genotype with each promoter). Significant interacting regions were determined for each replicate using w4CSeq (40), and each region shown in Fig. 8A was found in at least two replicates for each genotype. This analysis revealed that specific contacts are reproducibly lost while others are gained at these bidirectional promoters in *Rb1^{L/L}* MEFs in comparison to wild-type cells (Fig. 8A and B). In a number of instances, *Cdca3/Usp5* and *Pole/Pxmp2* showed similar changes in interactions between wild-type and *Rb1^{L/L}* fibroblasts. For example, the two bidirectional

FIG 4 Legend (Continued)

promoter. (E) The absolute values of the expression changes in the *Rb1* mutant MEFs versus those in *Rb1^{+/+}* MEFs from panel D are compared. The genes at CAP-D3-occupied bidirectional promoters were significantly more misexpressed in asynchronous *Rb1^{L/L}* MEFs than in either of the mutant MEFs grown under serum-starved conditions. (F) Heat maps of ChIP-Seq read abundances for histone tail modifications and RNA Pol2 in wild-type MEFs at the 1,271 1-kb promoter regions that contain a CAP-D3 peak. Heat maps are divided into promoters on the forward strand (top) and on the reverse strand (bottom). All error bars are ± 1 SEM; *, $P < 0.05$; one-way ANOVA.

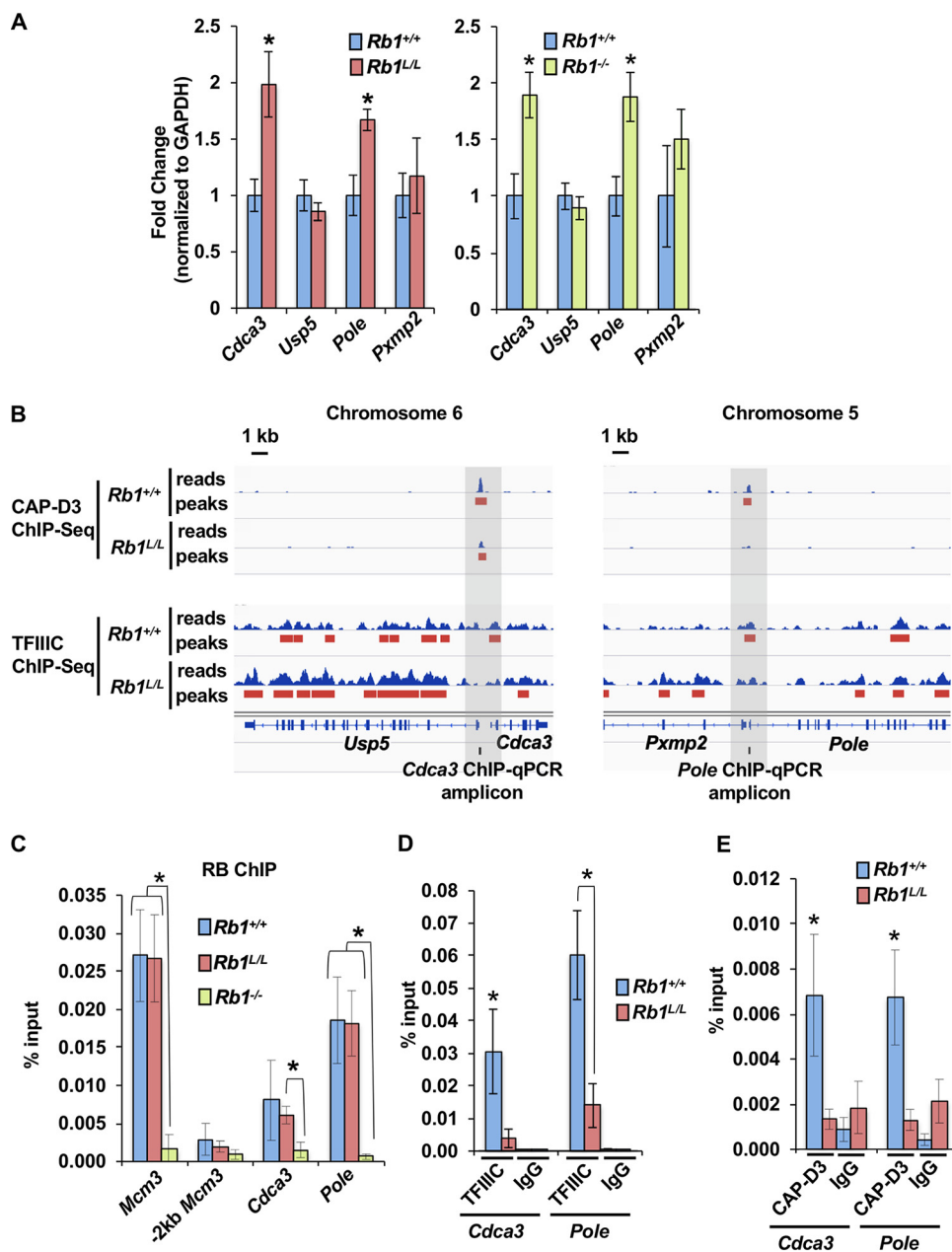


FIG 5 Bidirectional promoters are occupied by an RB-TFIIC-condensin II complex. (A) RT-qPCR of *Usp5/Cdca3* and *Pxmp2/Pole* bidirectional genes in *Rb1*^{+/+} and *Rb1*^{L/L} and in *Rb1*^{+/+} and *Rb1*^{-/-} MEF littermate pairs ($n = 5$). (B) *Usp5/Cdca3* and *Pxmp2/Pole* bidirectional promoter locations and their respective CAP-D3 and TFIIC ChIP-Seq reads and peaks in both *Rb1*^{+/+} and *Rb1*^{L/L} MEFs. All scales of read buildups are set to 35. (C) RB ChIP-qPCR results from asynchronously growing *Rb1*^{+/+}, *Rb1*^{L/L}, and *Rb1*^{-/-} MEFs at the bidirectional promoter locations indicated ($n = 5$). The *Mcm3* promoter and kb -2 upstream location are used as positive and negative controls, respectively, for RB ChIPs. (D) TFIIC ChIP-qPCR results from *Rb1*^{+/+} and *Rb1*^{L/L} MEFs at the same bidirectional promoter locations as described above ($n = 6$). (E) CAP-D3 ChIP-qPCR results from asynchronously growing *Rb1*^{+/+} and *Rb1*^{L/L} MEFs ($n = 5$). All error bars are ± 1 SEM. *, $P < 0.05$; determined by t test.

promoters contacted similar regions in chromosome 12, and Fig. 8C uses gray shading to illustrate a significantly contacted region found repeatedly in wild-type cells that was lost in all replicates of 4C-Seq in *Rb1*^{L/L} cells. Both *Cdca3/Usp5* and *Pole/Pxmp2* also gained common interactions on chromosome 4 in *Rb1*^{L/L} cells (Fig. 8D). Regions of the genome where contacts were independently lost from each viewpoint in *Rb1*^{L/L} cells compared to the wild type also occurred, and examples are shown in Fig. 8E and F. Collectively, these data reveal that statistically significant interactions are found between our chosen view-

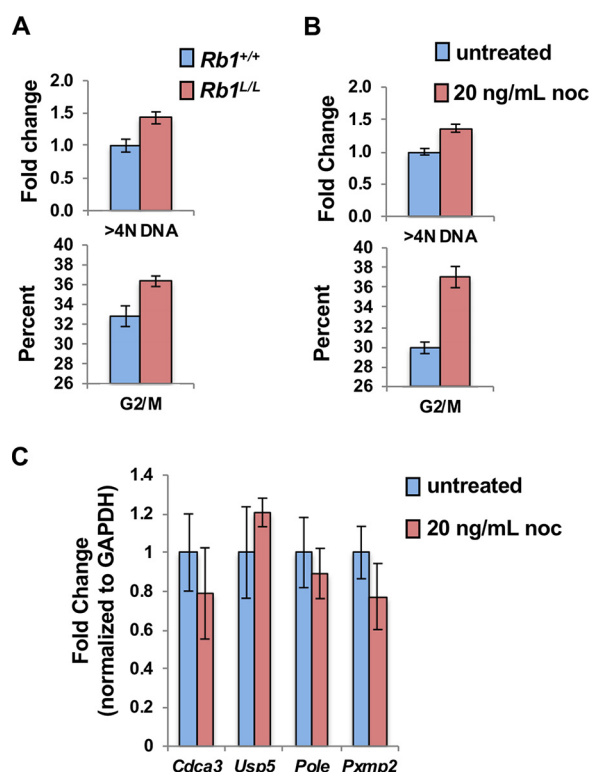


FIG 6 Gene expression at bidirectional promoters is not altered by microtubule inhibitor-induced aneuploidy. (A) Differences in >4N DNA content between *Rb1*^{+/+} and *Rb1*^{L/L} MEFs and percentage of cells in G₂/M as determined by propidium iodide (PI) staining and flow cytometry ($n = 6$). (B) *Rb1*^{+/+} MEFs were nocodazole (noc) treated for 24 h to increase the >4N DNA and the G₂/M content in wild-type MEFs similarly to the *Rb1*^{L/L} MEFs and the percentage of cells in G₂/M as determined by PI staining and flow cytometry ($n = 4$). (C) RT-qPCR was used to quantitate the expression of genes at the bidirectional promoters in untreated and nocodazole-treated *Rb1*^{+/+} cultures. All error bars are ± 1 SEM.

points and distant genome locations and that loss of these contacts is detected in chromatin from *Rb1*^{L/L} cells.

In order to understand the nature of long-range interactions that include our chosen locations, we utilized a previous 4C-Seq report that demonstrated that *Hoxa10*, used as a bait, interacts with a region 70 Mb away on chromosome 6 and includes the *Cdca3/Usp5* bidirectional promoter (41). Consistent with RB-condensin II complexes mediating these distant contacts, our ChIP-Seq data for CAP-D3 demonstrate that it is located at *Hoxa10* and that its recruitment is diminished by the *Rb1*^L mutation (Fig. 9A). ChIP-qPCR further reveals that RB localization is not changed between *Rb1*^{+/+} and *Rb1*^{L/L} MEFs at *Hoxa10* (Fig. 9B), but both CAP-D3 and TFIIC localization at *Hoxa10* are diminished in the *Rb1*^{L/L} genetic background (Fig. 9C and D). Furthermore, our 4C-Seq data using *Cdca3/Usp5* as the reference location reveals that *Hoxa10* interactions were detected in all four *Rb1*^{+/+} 4C-Seq replicates but in only one in *Rb1*^{L/L} cells (Fig. 9A). These data further support the observation that defective condensin II recruitment by RB can impact long-range chromosome interactions. In addition, our analysis demonstrates that *Rb1*^{L/L}-sensitive contacts can be detected from both chromosome locations involved in this interaction and that RB recruits condensin II to both sites.

Overall, chromatin conformations in *Rb1*^{L/L} MEFs are altered in comparison to the wild-type state, with interactions being both gained and lost. Furthermore, our analysis reveals changes in long-range interactions at both the *Cdca3/Usp5* and *Pole/Pxmp2* bidirectional promoters in *Rb1*^{L/L} cells rather than changes in local looping. This confirms a role for RB and condensin II in connecting bidirectional promoters with distant genomic contacts.

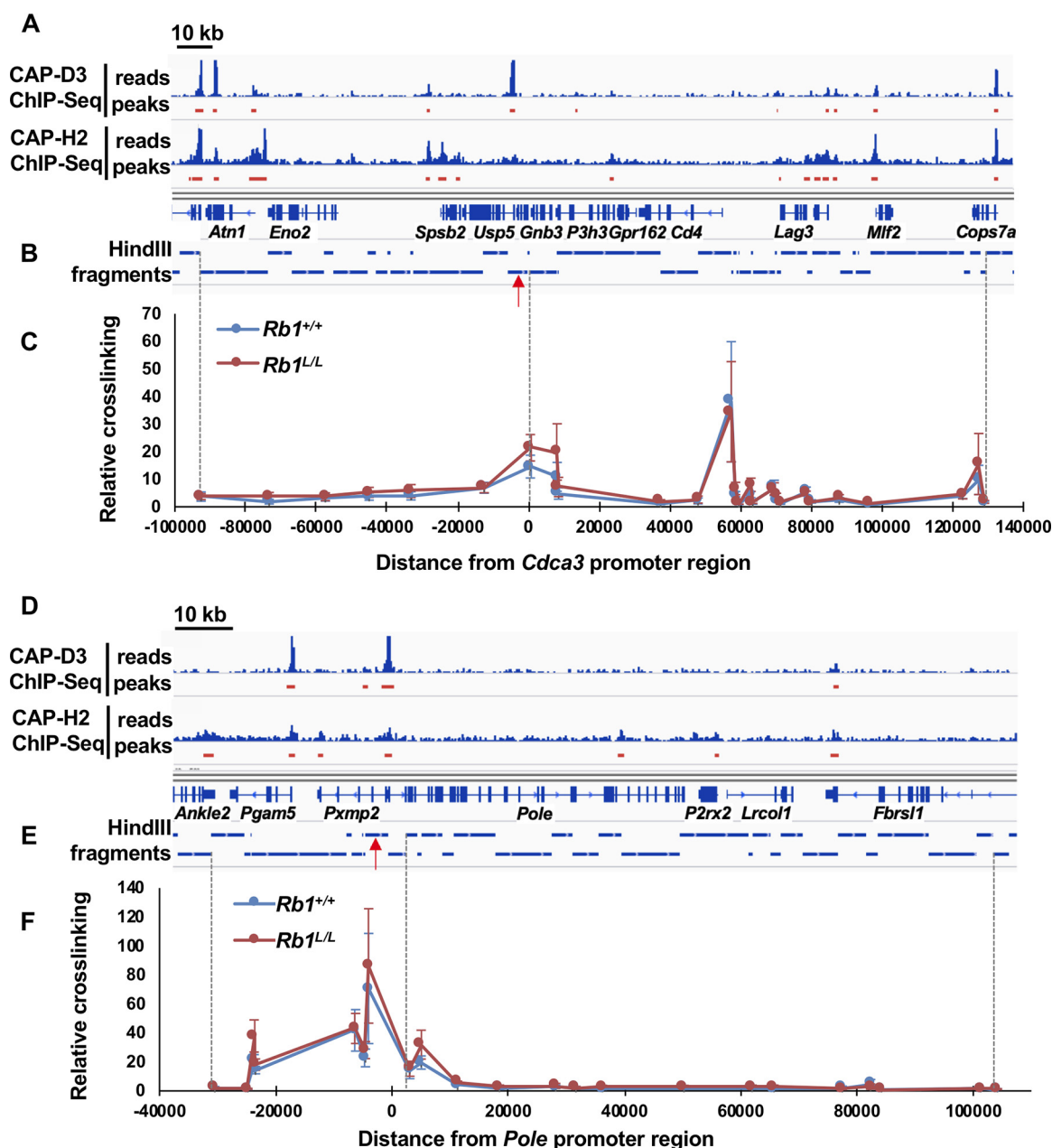


FIG 7 Preservation of 3C-detected chromatin loops in $Rb1^{L/L}$ cells. (A and D) CAP-D3 and CAP-H2 ChIP-Seq read tracks (EGS and formaldehyde fixed), surrounding the *Usp5/Cdca3* bidirectional promoter (A) and the *Pxmp2/Pole* locus (D). The read buildup scale is set to 50. (B and E) HindIII restriction enzyme fragments are shown as tracks in relation to the gene structure of these genomic locations. (C and F) 3C interaction frequencies for selected HindIII fragments (represented by dots) in the *Usp5/Cdca3* and *Pxmp2/Pole* regions of interest are displayed in graphical format. The dashed vertical lines relate restriction enzyme fragments to specific data points. The bait fragments are indicated by arrows. 3C cross-linking frequencies were normalized to the *Ercc3* locus ($n = 4$). All error bars are ± 1 SEM.

DISCUSSION

In order to study loss-of-function effects caused by defective condensin II chromatin loading in interphase, we utilized a targeted murine $Rb1^L$ mutant in which RB-condensin II interactions are impaired (20). Using ChIP-Seq and chromosome conformation capture approaches, we demonstrate that RB organizes chromosome architectural protein complexes TFIIC and condensin II in proximal-promoter regions of genes. In particular, bidirectional promoters are occupied by these proteins and they mediate long-range chromosome interactions. These data suggest that RB-TFIIC-condensin II occupancy of these genome locations acts as an architectural organizer that contrib-

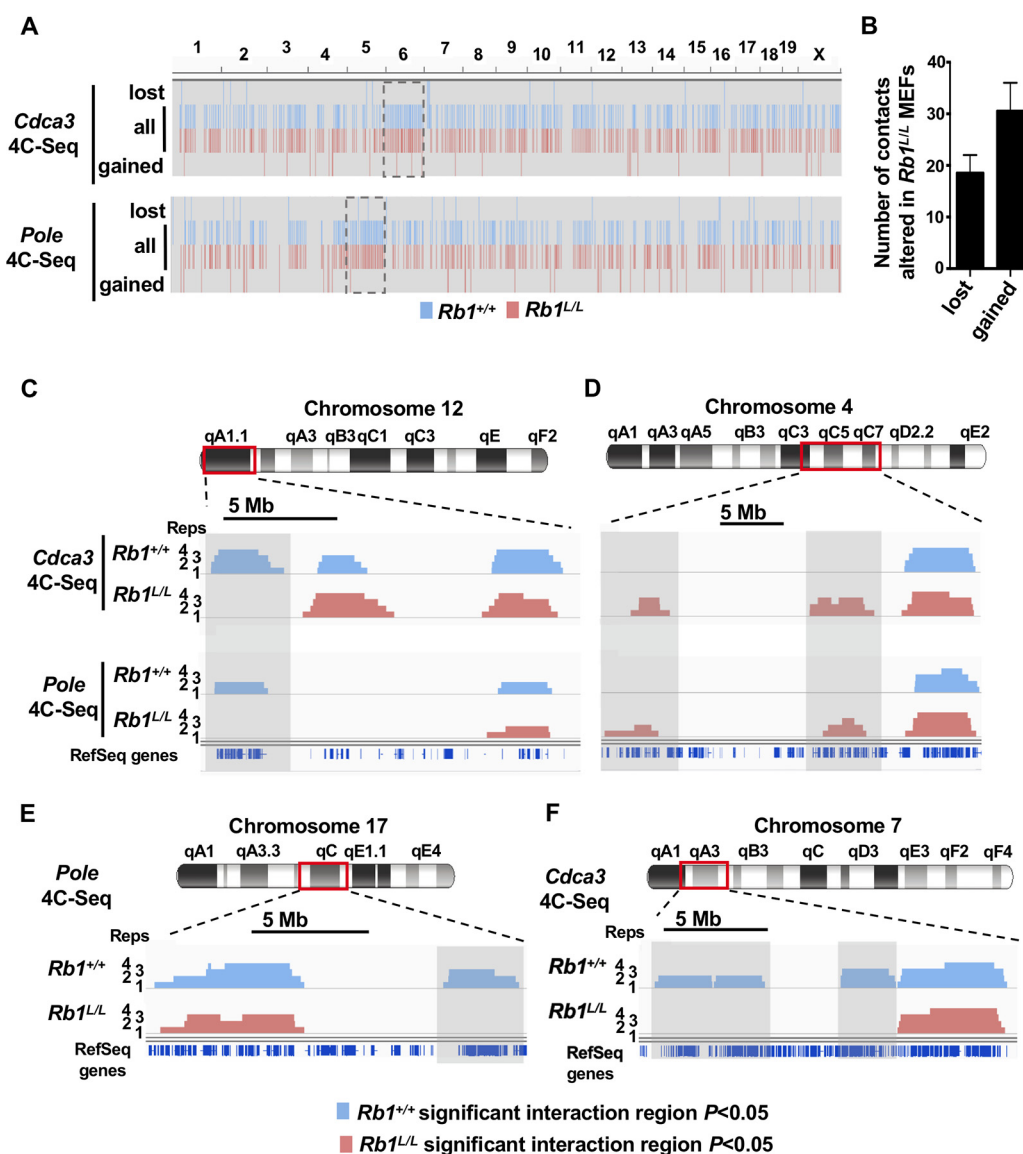


FIG 8 Loss of long-range chromosome contacts in *Rb1*^{L/L} MEFs. (A) 4C-Seq was used to determine chromosomal regions that interact with the *Usp5/Cdca3* and *Pxmp2/Pole* promoters. Statistically significant interacting regions were determined using w4CSeq for each of four different wild-type and *Rb1*^{L/L} replicates. Regions that were identified in two or more replicates are shown as red or blue bars, and chromosome positions are shown across the top. The complete set of regions identified in *Rb1*^{+/+} and in *Rb1*^{L/L} cells are labeled as “all,” while “lost” regions represent contacts identified in wild-type MEFs but absent in *Rb1*^{L/L} cells and “gained” regions represent novel contacts found only in *Rb1*^{L/L} cells from that viewpoint. (B) The numbers of 4C-Seq significant interacting regions, from panel A, found in wild-type MEFs and lost in *Rb1*^{L/L} MEFs (“lost”) or found in *Rb1*^{L/L} but not in wild-type MEFs (“gained”) at the *Cdca3* or the *Pole* viewpoints is shown. (C) Chromosome ideograms are used to depict regions of contact. Significantly contacting regions are represented by horizontal bars, with the height of each bar representing the number of experimental replicates (“Reps”) containing the interaction. An example of a lost contact that is common to *Cdca3* and *Pole* viewpoints is shown. (D) An example of new contacts formed in *Rb1*^{L/L} MEFs that are common to both viewpoints is shown. (E and F) Examples of a lost contact in *Rb1*^{L/L} MEFs from the *Pole* viewpoint (E) and from the *Cdca3* viewpoint (F) are shown.

utes to expression potential for closely spaced genes (Fig. 9E). Reduction of TFIIC and condensin II recruitment caused by the *Rb1*^L allele alters long-range contacts mediated from these locations, suggesting that altered chromosome topology may influence these gene expression patterns. We think that condensin II is the main contributor to the formation of these long-range chromosome interactions, although we cannot formally rule out that TFIIC may play a role.

The involvement of RB in TFIIC and condensin II recruitment to gene promoters in interphase may seem surprising. We note that some prior studies of mammalian

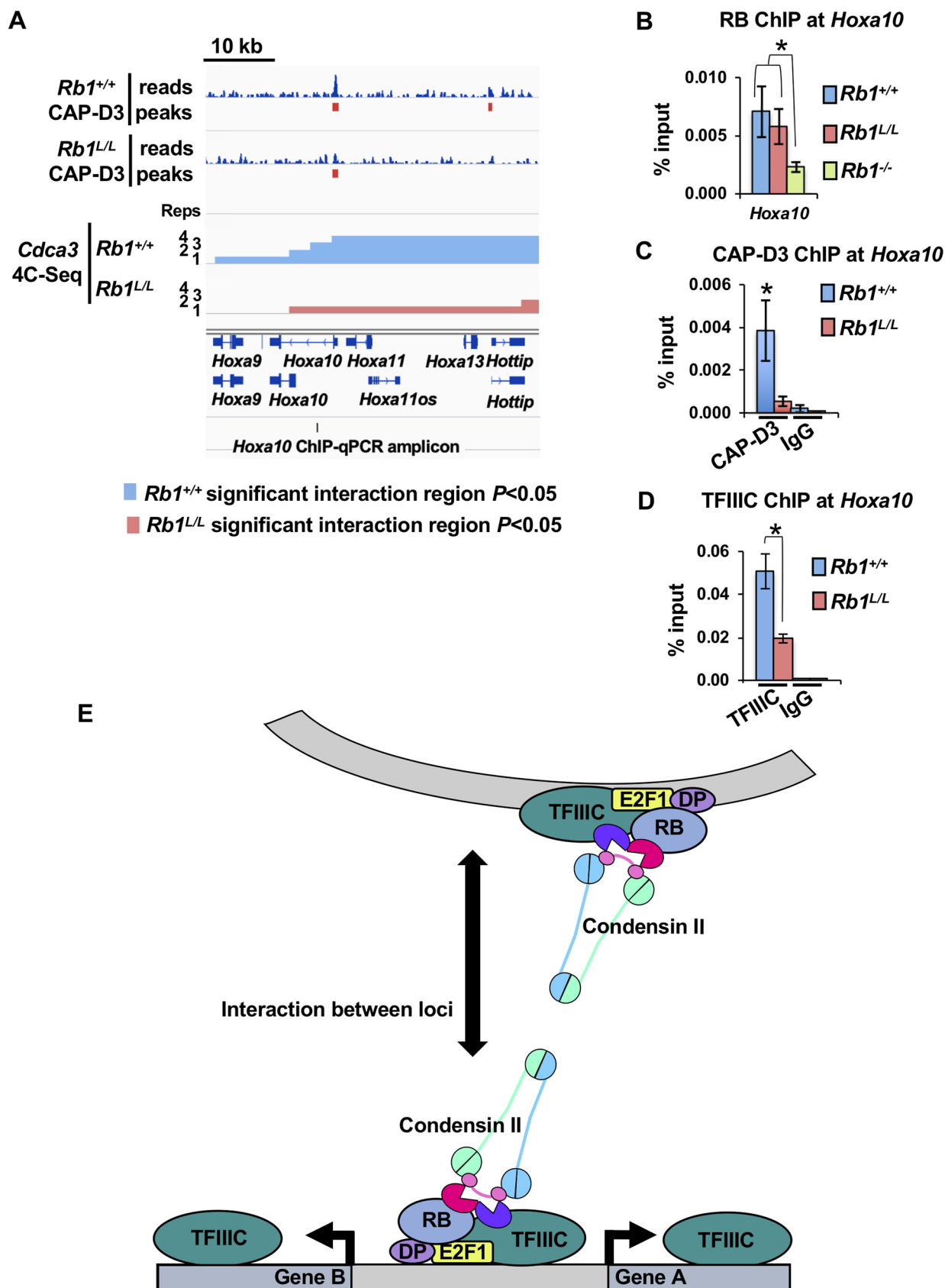


FIG 9 Changes in RB-condensin II complex binding correlate with altered interactions between the *Usp5/Cdca3* bidirectional promoter and the *Hoxa* locus. (A) Genome browser view of the *Hoxa* locus on chromosome 6 showing CAP-D3 ChIP-Seq reads and peaks from formaldehyde-

(Continued on next page)

condensin II have utilized cell lines that are transformed by viral oncogenes that target RB (13, 42). RB's role in organizing long-range contacts would likely be disrupted in these cells, or condensin II would rely on compensatory mechanisms to load in RB's absence. A number of previous studies have demonstrated that RB interacts with condensin II and that this interaction is conserved in *Drosophila* (28, 43). Furthermore, TFIIIC has previously been shown to bind to RB (44), indicating that these protein complexes have been known to function together, but their role in chromosome interactions and transcriptional control at divergent promoters was unknown (45).

The regional effects on transcript levels identified at bidirectional promoters in *Rb1^{L/L}* cells demonstrate an RB-dependent effect on gene upregulation but also down-regulation, suggesting that wild-type *Rb1* positively influences gene expression in these instances. Not only is this inconsistent with RB's historical role as a transcriptional repressor during cell cycle arrest, but it also indicates that RB creates small regional influences on expression akin to territories or compartments. This general organization of gene transcription territories has been proposed in other studies (46, 47). Furthermore, recent studies of chromosome topology indicate that functional compartments created by some long-range contacts are maintained upon degradation of CTCF or cohesin components (8–12). Our data suggest that RB-condensin II may contribute to cohesin-independent contacts by providing a distinct means of linking distant chromosomal regions. However, additional work will be necessary to relate RB-dependent bidirectional promoters to chromosome topology that is organized by these other factors.

Cancer genomic studies have revealed that *RB1* deletions are preferentially enriched in metastatic disease (48) or in acquired resistance to targeted therapeutic agents (49). These are scenarios where deregulated proliferation has already been established and suggest that *RB1* loss has additional contributions to cancer biology. DNA damage and genome instability phenotypes in cancer cells are known to be caused by *RB1* loss (50). In addition, work presented here suggests that disruption of chromosome contacts by reduced condensin II recruitment may have obligatory effects on gene expression patterns during cancer progression because of its dependence on RB.

MATERIALS AND METHODS

Cell culture. MEFs were prepared and cultured from embryonic day 13.5 (E13.5) embryos according to standard methods (51). *Rb1^{+/+}*, *Rb1^{-/-}*, *Rb1^{L/L}*, *E2f1^{+/+}*, and *E2f1^{-/-}* MEFs were genotyped as previously described and used by passage 4 (22).

ChIP. Chromatin immunoprecipitation (ChIP) was conducted according to protocols adapted from a report by Cecchini et al. (32). Briefly, asynchronously cycling cells were fixed in either 1% formaldehyde in 1× phosphate-buffered saline (PBS) or in 2 mM ethylene glycol bis(succinimidyl succinate) (EGS) in 1× PBS, followed by 1% formaldehyde. Both fixing reactions were neutralized with 0.125 M glycine. Cross-linked chromatin was sonicated so that most chromatin was ≤400 bp. Sheared chromatin was then normalized between experimental groups and precleared with protein G Dynabeads and IgG. Precleared chromatin was then incubated with protein G Dynabeads and ChIP antibodies to immunoprecipitate proteins. The following antibodies were used to precipitate proteins: anti-CAP-D3 (28), anti-CAP-H2 (A302-275A; Bethyl), anti-H3K27me3 (07-449; EMD Millipore), anti-RB (C-15; Santa Cruz), anti-RB (M-153; Santa Cruz), anti-RB (M-136 [32]), anti-RB (s855 [32]), anti-RB (Hyb4.1; Developmental Studies Hybridoma Bank), and anti-TFIIIC-220 (A301-291A; Bethyl). Cross-links were reversed at 65°C, and samples were treated with RNase and proteinase K. DNA was isolated for qPCR and/or library preparation.

For ChIP-qPCR, the following primer pairs were used: *Lmn2*-F, 5'-TCGGAGGCTCTATGGGAAAC-3', and *Lmn2*-R, 5'-AAGGACAGTCTTAGGACG-3'; *Cdca3*-F, 5'-TCTCTCGCATCAATGAGCG-3', and *Cdca3*-R, 5'-TACCCGCGCGCTTTTATT-3'; *Pole*-F, 5'-TCATTGGCCGAAGCCGTAG-3', and *Pole*-R, 5'-TTCC TCAGGACCATTGCGAC-3'; *Mcm3*-F, 5'-ATCCAGGAAGTCCAAGTAGTCTCTC-3', and *Mcm3*-R, 5'-TTGAAGTG

FIG 9 Legend (Continued)

fixed wild-type and *Rb1^{L/L}* MEFs displayed at the top (with the read buildup scale set to 20). 4C-Seq significant interacting regions from individual replicates ("Reps") of each genotype from the *Cdca3* 4C-Seq experiments are shown. The height of the bars indicates the number of replicates that had significant interaction with each region of the *Hoxa* locus. (B) RB ChIP-qPCR results from asynchronously growing *Rb1^{+/+}*, *Rb1^{L/L}*, and *Rb1^{-/-}* MEFs at the indicated location in *Hoxa10* ($n = 4$). (C) CAP-D3 ChIP-qPCR results from *Rb1^{+/+}* and *Rb1^{L/L}* MEFs at *Hoxa10* ($n = 4$). (D) TFIIIC ChIP-qPCR results from *Rb1^{+/+}* and *Rb1^{L/L}* MEFs at *Hoxa10* ($n = 4$). All error bars are ± 1 SEM. *, $P < 0.05$; determined by t test. (E) Model of RB-TFIIIC-condensin II-mediated long-range chromosome interactions between bidirectional promoters and distant loci. RB-TFIIIC-condensin II assembles at both bidirectional promoters as well as at distant interacting regions such as *Hoxa10*, but how these two complexes interact when forming long-range chromosome contacts is unknown.

GTTAGCCAATCATAACG-3'; Mcm3_-2kb-F, 5'-GCCAAGGCAAAACAACAATTCTAC-3', and Mcm3_-2kb-R, 5'-CTATCTCTTTGATTTTGGGTGGCTG-3'; Hist1h3b_F, 5'-GTCTGTTTGAGGACACCAACCT-3', and Hist1h3b_R, 5'-TTTGGGTCCAGTTTGCACCTTG-3'; and Hoxa10_F, 5'-ACTGGGGATCTCGGTCTAC-3', and Hoxa10_R, 5'-CAGATACTGGCGGTGTC-3'.

ChIP-Seq libraries and alignment. For ChIP-Seq, some previously published data were used for analysis. FASTQ reads were downloaded from the following data sets: CAP-D3 (GSE55040: GSM1328449, GSM1328450, and GSM1328448), Pol2 (GSE36027: GSM918740 and GSM918761), H3K4me1 (GSE31039: GSM769028 and GSM769030), H3K4me3 (GSE31039: GSM769029 and GSM769030), H3K27ac (GSE29218: GSM851277 and GSM723008), H3K27me3 (GSE77993: GSM2064311 and GSM2064301), H3K36me3 (GSE53939: GSM1303764 and GSM1303761), and H3K9me3 (GSE53939: GSM1303762 and GSM1303761) (20, 52–54). ChIP-Seq libraries created for this study occasionally used DNA from multiple ChIP replicates per genotype. For CAP-H2 and CAP-D3 ChIPs, 5 IP replicates were combined, and for H3K27me3 ChIPs, 2 IP replicates per library were used. ChIP libraries were sequenced using an Illumina NextSeq (high-output, 75-cycle kit).

All FASTQ reads (both from ChIP-Seq data published for other studies and from ChIP-Seq data obtained for this study) were aligned to mouse genome build mm9 using Bowtie2 version 2.3.0 (55). Reads aligning to multiple locations of a particular element were distributed randomly to these positions, while multiple reads mapping to the same location were retained as previously described (56). The following command was used: bowtie2 -t -p 4 -D 15 -R 2 -L 32 -i S,1,0.75 -x mm9 -U <reads>.fastq -S <output>.sam.

Peak calling and annotation. Peaks were identified using MACS version 1.4.0rc2 according to the parameters stated below (26). The following command was used: macs14 -t <ChIP>.sam -c <input>.sam -n <output> -g mm -B -S. For analysis of CAP-D3 localization, only peak locations that had 10 or more tags, a *P* value of at most 10^{-5} , and a fold enrichment of at least 4 were used for subsequent analyses. Reads and peak locations were visualized using Integrative Genomics Viewer (IGV) (57, 58).

Peak enrichment per genomic region was determined using CEAS and the mm9 RefSeq table supplied with the program (27). To determine the number and significance of peaks overlapping with other peaks or genomic elements, BEDTools was used (59, 60).

To create heat maps of reads, bamCoverage was first used to generate normalized bigWig files of ChIP and input reads using reads per genomic content (RPGC; $1 \times$ normalization), followed by bigwig-Compare to subtract the normalized input signal from the ChIP signal (61, 62). computeMatrix was then used to calculate read enrichment scores at promoters with wild-type CAP-D3 peaks, and plotHeatmap was used to plot those scores.

Functional annotation of genes of interest was performed using the Database for Annotation, Visualization and Integrated Discovery (DAVID) (30). Genes were submitted to DAVID and analyzed using the functional annotation tool with the following categories selected: GOTERM_BP_DIRECT, GOTERM_CC_DIRECT, GOTERM_MF_DIRECT, UP_KEYWORDS, UP_SEQ_FEATURE, KEGG_PATHWAY, BIOCARTA, INTERPRO, PIR_SUPERFAMILY, and SMART. Functional annotation clustering was then used to cluster all of the gene enrichment results, with default parameters. The enrichment score for the annotation clusters represents the geometric mean, in $-\log$ scale, of the members' *P* values in each corresponding annotation cluster. Functional annotation clusters were manually described based on their overarching theme.

Immunoprecipitation. Chromatin fractionation was conducted using methods previously reported by Ishak et al. (53). These DNase I-prepared chromatin fractions from asynchronously cycling cells were used for immunoprecipitation. Briefly, proteins were first precleared using protein G Dynabeads and mouse IgG before overnight precipitation using an anti-RB antibody (clone G3-245; BD Pharmingen). Protein G Dynabeads were added to the immunoprecipitation mixtures the next day and rocked for another 2 h. Proteins were resolved by SDS-PAGE, followed by Western blotting using standard techniques. The following antibodies were used for Western blotting: anti-CAP-D3 (28), anti-SMC2 (20), and anti-RB (clone G3-245; BD Pharmingen).

RNA-Seq. Total RNA from proliferating MEFs was isolated using TRIzol reagent according to the standard protocol (Invitrogen). Three *Rb1*^{+/+} and *Rb1*^{L/L} MEF pairs were used for this analysis. All samples were further processed and sequenced at the London Regional Genomics Centre (Robarts Research Institute, London, Ontario, Canada; <http://www.lrgc.ca>). Total RNA samples were quantified using the Qubit 2.0 fluorometer (Thermo Fisher Scientific), and quality was assessed using the Agilent 2100 bioanalyzer (Agilent Technologies, Inc.) and the RNA 6000 nano kit (Caliper Life Sciences). They were then processed using the ScriptSeq complete gold kit (H/M/R) (Illumina, Inc.), which includes Ribo-Zero rRNA removal. Samples were fragmented, and cDNA was synthesized, tagged, cleaned up, and subjected to PCR with indexed reverse primers (ScriptSeq index PCR primers) to permit equimolar pooling of samples into one library. Samples were sequenced on an Illumina NextSeq 500 (mid-output, 150-cycle kit). FASTQ data files were then downloaded from BaseSpace.

For alignment of reads, a STAR v2.5.0a aligner was used (63). To generate a genome index, the mm9 chromFa.tar.gz file was downloaded from UCSC to create mm9_full_genome.fa, and the following command was used: STAR --runThreadN 4 --runMode genomeGenerate --genomeDir <STAR_genome_indices_directory> --genomeFastaFiles mm9_full_genome.fa --genomeSAsparseD 2 --limitGenomeGenerateRAM 2000000000 (64). For the alignments, the following STAR command was used: STAR --runMode alignReads --runThreadN 8 --genomeDir <STAR_genome_indices_directory> --readFilesIn <reads>.fastq --sjdbGTFfile mm9_UCSC_knownGene.gtf --sjdbOverhang 149 --sjdbInsertSave All --outSAMtype BAM Unsorted SortedByCoordinate --outFileNamePrefix <output> --outReadsUnmapped Fastx --outMultimapperOrder Random --outSAMattributes NH HI AS NM XS --outWigType wiggle. StringTie v1.3.2 was then used to assemble RNA-Seq alignments into potential transcripts with the following command: stringtie <STAR_

aligned_sample>.sortedByCoord.out.bam -o <output>.gtf -p 4 -G mm9_UCSC_knownGene.gtf -A <output>_gene_abund.tab -B -e (65). The prepDE.py script provided with StringTie was then utilized to extract read count information from the generated files, and DESeq2 was used to determine differential gene expression between *Rb1*^{+/+} and *Rb1*^{L/L} genotypes. When overall gene expression was analyzed, all normalized transcript read counts from DESeq2 were summed for each gene and the average results for the three *Rb1*^{L/L} MEF preparations were compared to the average results for three wild-type MEFs. Genes from bidirectional promoters that had normalized read counts of less than 1 for any of the samples were excluded from heat maps of data, which were created using matrix2png (66).

Expression microarray analysis. Total RNA from proliferating MEFs was isolated using TRIzol reagent according to the standard protocol (Invitrogen). Samples were labeled and processed for GeneChips at the London Regional Genomics Centre (Robarts Research Institute, London, Ontario, Canada). Three *Rb1*^{+/+} and *Rb1*^{L/L} MEF pairs were used with biotin end-labeled single-strand cDNA with the Affymetrix GeneChip WT Plus reagent kit. A 5.5- μ g amount of end-labeled cDNA was hybridized for 16 h at 45°C on GeneChip mouse gene 1.0 ST arrays that were subsequently washed, stained by a GeneChip fluidics station 450, and scanned using the Affymetrix GeneChip scanner 3000 7G using Command Console v3.2.4. Robust multiarray average (RMA) expression values derived from CEL files were log transformed prior to analysis of variance (ANOVA) using the Partek Genomics Suite. Annotations were derived from Affymetrix MoGene-1_0-st-v1 transcript cluster annotations, CSV, release 32. Heat maps of expression values were created using matrix2png (66).

Data from expression microarray experiments for serum-starved MEFs can be found in GEO under the following accession numbers: [GSE85638](#), *Rb1*^{L/L} versus the wild type, and [GSE54924](#), *Rb1*^{G/G} versus the wild type.

Comparison of transcriptome analysis and ChIP-Seq data. To compare CAP-D3 ChIP-Seq binding sites to changes in transcription, BETA was used (31). First, RNA-Seq data were converted to BETA-specific format (BSF) with the fold change values being reported as wild type versus *Rb1*^{L/L} so that expression changes when CAP-D3 could bind were highlighted. The expression data were then compared to the filtered list of high-confidence CAP-D3 peaks (see above) using BETA, taking into account CTCF binding sites using the following command: BETA plus -p <CAP-D3_peaks>.bed -e <expression_changes>.txt -k BSF -bl -g mm9 -gs mm9.fa -n <output>.

qRT-PCR analysis of expression. Total RNA from proliferating MEFs was isolated using TRIzol reagent according to the standard protocol (Invitrogen). First-strand cDNA synthesis was performed using random primers, RNaseOUT, and SuperScript III reverse transcriptase according to manufacturer's instructions (Invitrogen). Isolated cDNA was used in qRT-PCRs with iQ SYBR green supermix (Bio-Rad) with the following primers: *Cdca3*_exp_F, 5'-GTAGCAGACCCTCGTTCACC-3'; *Cdca3*_exp_R, 5'-ATCCGACGCTTCTGTCTCC-3'; *Usp5*_exp_F, 5'-ATGGCGGAGCTGAGTGAAGA-3'; *Usp5*_exp_R, 5'-ATAGAGGCCACCCTCAGACT-3'; *Pole*_exp_F, 5'-GAGAAGGTGCTGTGGAACA-3'; *Pole*_exp_R, 5'-GCTGTAGGCGTTGGTAAGA-3'; *Pxmp2*_exp_F, 5'-GACTGCTAGCTGTTGGGTG-3'; *Pxmp2*_exp_R, 5'-CCAAGGGCTGACAAATGCC-3'; *GAPDH*_exp_F, 5'-GCACA GTCAAGGCCGAGAAT-3'; and *GAPDH*_exp_R, 5'-GCCTTCTCCATGGTGGTGAA-3'. Resulting target quantification cycle (*C_q*) values were normalized to *GAPDH* (glyceraldehyde-3-phosphate dehydrogenase) and then expressed as a fold change relative to the mean for the global wild type.

Flow cytometry. Cells were plated on 10-cm plates at a density of 900,000 cells per plate. Approximately 24 h later, cells were pulsed with BrdU for a duration of 2 h. Cell cycle analysis was then carried out as previously described (67).

Nocodazole treatment. Cells were plated on 10-cm plates at a density of 900,000 cells per plate or on 6-cm plates at a density of 300,000 cells per plate. Approximately 24 h after seeding, cell medium was replaced with standard culture medium containing either dimethyl sulfoxide (DMSO) only (control) or 20 ng/ml nocodazole. One day after treatment with nocodazole, the cells were processed for flow cytometry and qRT-PCR expression analysis (see above).

3C analysis. Chromosome conformation capture (3C) analysis was conducted according to protocols adapted from a report by Hagège et al. (68). Briefly, cells were trypsinized, centrifuged, and resuspended to make a single-cell suspension, followed with cross-linking in 1% formaldehyde–10% FCS/PBS. The reactions were quenched with glycine, and the cells were then pelleted and lysed in 5 ml cold lysis buffer (50 mM Tris-HCl [pH 7.5], 150 mM NaCl, 5 mM EDTA, 0.5% NP-40, 1% Triton X-100, and protease inhibitors). Samples were digested with HindIII, ligated using T4 DNA ligase, and treated with proteinase K, and cross-links were reversed at 65°C. Samples were then treated with RNase A, followed by phenol-chloroform purification. 3C samples were digested with a second restriction enzyme, EcoRI, to help minimize potential PCR biases resulting from limited template accessibility. The resulting final 3C products were quantified in triplicate by quantitative TaqMan real-time PCR after 3C DNA was normalized to a final concentration of 50 ng/ μ l. Bacterial artificial chromosomes (BACs), clones RP23-333M22 and RP23-55K5, containing the *Pxmp2*/*Pole* and *Cdca3*/*Usp5* bidirectional promoters of interest, respectively, were used as control templates. To generate random ligation products of HindIII fragments at the regions of interest, BACs were individually digested with HindIII, ligated, and digested again with EcoRI. This ligated BAC DNA was serially diluted and used to generate standard curves in each qPCR run for each primer pair to which all 3C products were normalized. The 3C signals at each locus were further normalized to those from a control locus, ERCC3, with primers and a probe described previously (69). Probe and primer sequences are as follows (primer names correspond to approximate position [in kb] relative to bidirectional promoters): *Cdca3*_const, 5'-TAGAGCAAAGCTACACCGGG-3'; *Cdca3*_Probe, 5'-FAM-AGAGAGATCTATCCAGGTCTCACAGGCC-TAMRA-3'; *Cdca3*_-93, 5'-GACCACTGCGAGACGGAAG-3'; *Cdca3*_-73, 5'-CCCCAGATACACTAATCCCTG-3'; *Cdca3*_-57, 5'-CCTCTCCCTCTTTCTTCC-3'; *Cdca3*_-45, 5'-TACAGATGGTTGCGAGGCAC-3'; *Cdca3*_-33, 5'-GCTGGGAGGATGAGAAAAATGAC-3'; *Cdca3*_-13, 5'-ATCCAGAGATTCACGCTTGTCT-3'; *Cdca3*_+1, 5'-CCTGGAGGAGGCCATTCAAG-3'; *Cdca3*_+8, 5'-CCAAG

TCTACCATCTCGGGG-3'; *Cdca3*₊₉, 5'-TTGGGTGACTGAGATAGCCC-3'; *Cdca3*₊₃₇, 5'-CCTGGCACACAGCAA GC-3'; *Cdca3*₊₄₈, 5'-ACCAGAACAGACATCTCAAGTAACA-3'; *Cdca3*₊₅₇, 5'-TGCATAGCGATGGGTTTCACA-3'; *Cdca3*₊₅₉, 5'-TGGCCAGAATGACTGCAAGAA-3'; *Cdca3*₊₆₃, 5'-CCCTCTCCAGGGTAAAGC-3'; *Cdca3*₊₆₄, 5'-GTTCCAGAACTTCTCTCTTTGC-3'; *Cdca3*₊₆₉, 5'-GAGGCATGCCACGTAAGC-3'; *Cdca3*₊₇₀, 5'-CCCGCAGGAGAGGGACTAAA-3'; *Cdca3*₊₇₁, 5'-TCGGAATTTGCTCCAGAGTC-3'; *Cdca3*₊₇₉, 5'-GTGGG GACAGTAGAGGAAGC-3'; *Cdca3*₊₈₀, 5'-GCTGAGCCAGTGGAAAG-3'; *Cdca3*₊₈₈, 5'-GGCTCTGTTACCAC AACTGTC-3'; *Cdca3*₊₉₆, 5'-AGAAGCTGACTTGGGCTACAT-3'; *Cdca3*₊₁₂₃, 5'-GTCTAACGGTTGGTAGAGT GG-3'; *Cdca3*₊₁₂₇, 5'-ACATAATAACACAGGGGCCG-3'; *Cdca3*₊₁₂₉, 5'-CACTGACTGACGCACAGAAGAA-3'; *Pole*_{const}, 5'-GGTGTCTCTGCTGCCAAGG-3'; *Pole*_{Probe}, 5'-FAM-TGCTCCGGCCGCGGTAC-TAMRA-3'; *Pole*₋₃₀, 5'-ACAGCCAGAACTACACAGAGG-3'; *Pole*₋₂₅, 5'-ACTGTTGTGGACTGATGCTTAGAA-3'; *Pole*₋₂₄, 5'-TGCCCTGTCTGAAGTCTGC-3'; *Pole*₋₂₃, 5'-CTCAGGAGACAGGCAAGCTAA-3'; *Pole*₋₆, 5'-ATGGCAATCACAG GCACAAG-3'; *Pole*₋₅, 5'-CTGTCTCATCTGTGCCCTC-3'; *Pole*₋₄, 5'-TGCCAAAGTATGGGGGATGTG-3'; *Pole*₊₃, 5'-TTCCTCGGTGGGCATTCTC-3'; *Pole*₊₅, 5'-AGAAGATTGTGATCAGTGTCTTGA-3'; *Pole*₊₁₁, 5'-CTTGTGAACCTCTGCTCTTGC-3'; *Pole*₊₁₈, 5'-CTAATGGAACCGAGGAGCCG-3'; *Pole*₊₂₈, 5'-GCAATACACA AACGCTCTTGGTC-3'; *Pole*₊₃₂, 5'-AGCCAGACCAACCACTCTC-3'; *Pole*₊₃₆, 5'-TGAGAGTTGCTCTGTATGGA ACG-3'; *Pole*₊₅₀, 5'-AAAATGCCACCTTGCTGTG-3'; *Pole*₊₆₂, 5'-TTCAGGGTCTCTCTTTGGGAGTG-3'; *Pole*₊₆₆, 5'-GTGTTCTTCCTGTGTATATACCTTGC-3'; *Pole*₊₇₇, 5'-CTCCCTAAGTTTGCGGGCT-3'; *Pole*₊₈₂, 5'-TGGAGGAATGTGACTGGGA-3'; *Pole*₊₈₄, 5'-CTGGGCGCTTGGAGTTTAC-3'; *Pole*₊₁₀₁, 5'-TTGAAGCC TAGGTGGGAGTCTT-3'; *Pole*₊₁₀₄, 5'-ACAGGAGAGAGGCAGGTATGTC-3'; *ERCC3*₁, 5'-GCCCTCCCTGAAAAT AAGGA-3'; *ERCC3*₂, 5'-GACTTCTACCTGGGCTACA-3'; and *ERCC3*_{Probe}, 5'-FAM-AAAGCTTGACCTGCT TTAGTGGCC-TAMRA-3'.

4C-Seq. Samples were fixed, digested with HindIII, and ligated, and cross-links were reversed as detailed in the 3C protocol above. To generate circularized chromosome conformation capture (4C) products, 3C products were processed according to protocols adapted from a report by Splinter et al. (70). Briefly, 3C products were digested with NlaIII, ligated with T4 DNA ligase, and purified. Primers were designed for the bidirectional promoters of interest for inverse PCRs. For Illumina sequencing, all reading primers started with an Illumina read adapter sequence, 5'-AATGATACGGCGACCAACGAGATCTACACAC ACTCTTCCCTACACGACGCTCTCCGATCT-3', followed by a unique tag that was 0 to 3 nucleotides in length. These tags were unique to each sample and were used both to ensure that the nucleotide content for every cycle of sequencing was not the same (despite the use of the same primer sequence for all samples at the same viewpoint) and to pool multiple samples together. After the tag, the reading primers contained sequence unique to the viewpoint of interest, as close as possible to the HindIII digestion site. For the *Pole/Pxmp2* bidirectional promoter, this sequence was 5'-GATTCACCTCAAACCTCC ACAAAA-3', and for the *Cdca3/Usp5* bidirectional promoter, it was 5'-AGCAAGAGAGTGTAGCTAAG-3'. For the reverse sequencing primers for these viewpoints, the primers again started with an Illumina adapter sequence, 5'-CAAGCAGAAGACGGCATACGAGAT-3', followed by a sequence unique to the viewpoint of interest, close to the NlaIII restriction sites. For the *Pole/Pxmp2* bidirectional promoter, this sequence was 5'-TCCAAAGGATATATGAGGTTTCG-3', and for the *Cdca3/Usp5* bidirectional promoter, it was 5'-GTCTGA CTTGAGTTTTTCAG-3'. 4C product for sequencing was then prepared using Expand long template polymerase (Roche) and 3.2 µg of 4C template split between 16 PCRs. PCRs were pooled after completion and purified. 4C PCR products were then pooled in an equimolar fashion into one library and sequenced on an Illumina NextSeq (midoutput, 150-cycle kit).

Sequence reads were first trimmed to 20 bp total after the primer and bait sequence (excluding the HindIII site) using the FASTQ trimmer from the FASTX-Toolkit (http://hannonlab.cshl.edu/fastx_toolkit/). w4CSeq was then used to identify 4C sites and statistically significant regions and to look at intra- and interchromosomal interactions (40). For this analysis, the mm9 genome was used, a total of 500 enzyme sites was selected as the bin size for *trans* chromosomes (size_inter), a total of 100 enzyme sites was selected as the bin size for *cis* chromosomes (size_intra), a total of 3,000 enzyme sites was selected as the background window size for the *cis* chromosome (window_intra), and 0.05 was used as the false discovery rate (FDR) threshold. To compare the similarities of significant interacting regions, BEDTools Jaccard was used (59, 60). BEDTools merge was used to combine the significant interacting regions from each replicate for each viewpoint, and BEDTools intersect was run to determine the merged regions that were the same between genotypes.

Data availability. Data from RNA-Seq, ChIP-Seq, 4C-Seq, and expression microarrays that have not been published previously have been deposited in the GEO database (accession number [GSE125149](#)).

ACKNOWLEDGMENTS

We thank numerous colleagues for discussions and encouragement over the course of this study.

A.E.M. was a recipient of fellowship support from NSERC and OGS. This work was supported by funding from the CIHR (MOP 324579). F.A.D. is the Wolfe Senior Fellow in Tumor Suppressor Genes at Western University.

The funders had no role in study design, data collection and interpretation, or the decision to submit the work for publication.

REFERENCES

- Misteli T. 2007. Beyond the sequence: cellular organization of genome function. *Cell* 128:787–800. <https://doi.org/10.1016/j.cell.2007.01.028>.
- Rowley MJ, Corces VG. 2018. Organizational principles of 3D genome architecture. *Nat Rev Genet* 19:789–800. <https://doi.org/10.1038/s41576-018-0060-8>.
- Stadhouders R, Filion GJ, Graf T. 2019. Transcription factors and 3D genome conformation in cell-fate decisions. *Nature* 569:345–354. <https://doi.org/10.1038/s41586-019-1182-7>.
- Fraser J, Williamson I, Bickmore WA, Dostie J. 2015. An overview of genome organization and how we got there: from FISH to Hi-C. *Microbiol Mol Biol Rev* 79:347–372. <https://doi.org/10.1128/MMBR.00006-15>.
- van Ruiten MS, Rowland BD. 2018. SMC Complexes: universal DNA looping machines with distinct regulators. *Trends Genet* 34:477–487. <https://doi.org/10.1016/j.tig.2018.03.003>.
- Hirano T. 2016. Condensin-based chromosome organization from bacteria to vertebrates. *Cell* 164:847–857. <https://doi.org/10.1016/j.cell.2016.01.033>.
- Gibcus JH, Samejima K, Goloborodko A, Samejima I, Naumova N, Nuebler J, Kanemaki MT, Xie L, Paulson JR, Earnshaw WC, Mirny LA, Dekker J. 2018. A pathway for mitotic chromosome formation. *Science* 359:eaao6135. <https://doi.org/10.1126/science.aao6135>.
- Nora EP, Goloborodko A, Valton AL, Gibcus JH, Uebersohn A, Abdennur N, Dekker J, Mirny LA, Bruneau BG. 2017. Targeted degradation of CTCF decouples local insulation of chromosome domains from genomic compartmentalization. *Cell* 169:930–944.e22. <https://doi.org/10.1016/j.cell.2017.05.004>.
- Rao SSP, Huang SC, Glenn St Hilaire B, Engreitz JM, Perez EM, Kieffer-Kwon KR, Sanborn AL, Johnstone SE, Bascom GD, Bochkov ID, Huang X, Shamim MS, Shin J, Turner D, Ye Z, Omer AD, Robinson JT, Schlick T, Bernstein BE, Casellas R, Lander ES, Aiden EL. 2017. Cohesin loss eliminates all loop domains. *Cell* 171:305–320.e24. <https://doi.org/10.1016/j.cell.2017.09.026>.
- Schwarzer W, Abdennur N, Goloborodko A, Pekowska A, Fudenberg G, Loe-Mie Y, Fonseca NA, Huber W, C HH, Mirny L, Spitz F. 2017. Two independent modes of chromatin organization revealed by cohesin removal. *Nature* 551:51–56. <https://doi.org/10.1038/nature24281>.
- Wutz G, Varnai C, Nagasaka K, Cisneros DA, Stocsits RR, Tang W, Schoenfelder S, Jessberger G, Muhar M, Hossain MJ, Walther N, Koch B, Kueblbeck M, Ellenberg J, Zuber J, Fraser P, Peters JM. 2017. Topologically associating domains and chromatin loops depend on cohesin and are regulated by CTCF, WAPL, and PDS5 proteins. *EMBO J* 36:3573–3599. <https://doi.org/10.15252/emboj.201798004>.
- Haarhuis JH, van der Weide RH, Blomen VA, Yanez-Cuna JO, Amendola M, van Ruiten MS, Krijger PHL, Teunissen H, Medema RH, van Steensel B, Brummelkamp TR, de Wit E, Rowland BD. 2017. The cohesin release factor WAPL restricts chromatin loop extension. *Cell* 169:693–707.e14. <https://doi.org/10.1016/j.cell.2017.04.013>.
- Yuen KC, Slaughter BD, Gerton JL. 2017. Condensin II is anchored by TFIIIC and H3K4me3 in the mammalian genome and supports the expression of active dense gene clusters. *Sci Adv* 3:e1700191. <https://doi.org/10.1126/sciadv.1700191>.
- Van Bortle K, Nichols MH, Li L, Ong CT, Takenaka N, Qin ZS, Corces VG. 2014. Insulator function and topological domain border strength scale with architectural protein occupancy. *Genome Biol* 15:R82. <https://doi.org/10.1186/gb-2014-15-5-r82>.
- Cho SW, Xu J, Sun R, Mumbach MR, Carter AC, Chen YG, Yost KE, Kim J, He J, Nevins SA, Chin SF, Caldas C, Liu SJ, Horlbeck MA, Lim DA, Weissman JS, Curtis C, Chang HY. 2018. Promoter of lncRNA gene PVT1 is a tumor-suppressor DNA boundary element. *Cell* 173:1398–1412.e22. <https://doi.org/10.1016/j.cell.2018.03.068>.
- Betancur PA, Abraham BJ, Yiu YY, Willingham SB, Khameneh F, Zarnegar M, Kuo AH, McKenna K, Kojima Y, Leeper NJ, Ho P, Gip P, Swigut T, Sherwood RI, Clarke MF, Somlo G, Young RA, Weissman IL. 2017. A CD47-associated super-enhancer links pro-inflammatory signalling to CD47 upregulation in breast cancer. *Nat Commun* 8:14802. <https://doi.org/10.1038/ncomms14802>.
- Lupianez DG, Kraft K, Heinrich V, Krawitz P, Brancati F, Klopocki E, Horn D, Kayserili H, Opitz JM, Laxova R, Santos-Simarro F, Gilbert-Dussardier B, Wittler L, Borschiwer M, Haas SA, Osterwalder M, Franke M, Timmermann B, Hecht J, Spielmann M, Visel A, Mundlos S. 2015. Disruptions of topological chromatin domains cause pathogenic re-wiring of gene-enhancer interactions. *Cell* 161:1012–1025. <https://doi.org/10.1016/j.cell.2015.04.004>.
- Flavahan WA, Drier Y, Liao BB, Gillespie SM, Venteicher AS, Stemmer-Rachamimov AO, Suvà ML, Bernstein BE. 2016. Insulator dysfunction and oncogene activation in IDH mutant gliomas. *Nature* 529:110–114. <https://doi.org/10.1038/nature16490>.
- Herrera RE, Chen F, Weinberg RA. 1996. Increased histone H1 phosphorylation and relaxed chromatin structure in Rb-deficient fibroblasts. *Proc Natl Acad Sci U S A* 93:11510–11515. <https://doi.org/10.1073/pnas.93.21.11510>.
- Coschi CH, Ishak CA, Gallo D, Marshall A, Talluri S, Wang J, Cecchini MJ, Martens AL, Percy V, Welch I, Boutros PC, Brown GW, Dick FA. 2014. Haploinsufficiency of an RB-E2F1-Condensin II complex leads to aberrant replication and aneuploidy. *Cancer Discov* 4:840–853. <https://doi.org/10.1158/2159-8290.CD-14-0215>.
- Ishak CA, Coschi CH, Roes MV, Dick FA. 2017. Disruption of CDK-resistant chromatin association by pRB causes DNA damage, mitotic errors, and reduces Condensin II recruitment. *Cell Cycle* 16:1430–1439. <https://doi.org/10.1080/15384101.2017.1338984>.
- Isaac CE, Francis SM, Martens AL, Julian LM, Seifried LA, Erdmann N, Binne UK, Harrington L, Sicinski P, Berube NG, Dyson NJ, Dick FA. 2006. The retinoblastoma protein regulates pericentric heterochromatin. *Mol Cell Biol* 26:3659–3671. <https://doi.org/10.1128/MCB.26.9.3659-3671.2006>.
- Talluri S, Isaac CE, Ahmad M, Henley SA, Francis SM, Martens AL, Bremner R, Dick FA. 2010. A G1 checkpoint mediated by the retinoblastoma protein that is dispensable in terminal differentiation but essential for senescence. *Mol Cell Biol* 30:948–960. <https://doi.org/10.1128/MCB.01168-09>.
- Bourgo RJ, Thangavel C, Ertel A, Bergseid J, McClendon AK, Wilkens L, Witkiewicz AK, Wang JY, Knudsen ES. 2011. RB restricts DNA damage-initiated tumorigenesis through an LXCXE-dependent mechanism of transcriptional control. *Mol Cell* 43:663–672. <https://doi.org/10.1016/j.molcel.2011.06.029>.
- Britigan EM, Wan J, Zasadil LM, Ryan SD, Weaver BA. 2014. The ARF tumor suppressor prevents chromosomal instability and ensures mitotic checkpoint fidelity through regulation of Aurora B. *Mol Biol Cell* 25:2761–2773. <https://doi.org/10.1091/mbc.E14-05-0966>.
- Zhang Y, Liu T, Meyer CA, Eeckhoutte J, Johnson DS, Bernstein BE, Nussbaum C, Myers RM, Brown M, Li W, Liu XS. 2008. Model-based analysis of ChIP-Seq (MACS). *Genome Biol* 9:R137. <https://doi.org/10.1186/gb-2008-9-9-r137>.
- Shin H, Liu T, Manrai AK, Liu XS. 2009. CEAS: cis-regulatory element annotation system. *Bioinformatics* 25:2605–2606. <https://doi.org/10.1093/bioinformatics/btp479>.
- Coschi CH, Martens AL, Ritchie K, Francis SM, Chakrabarti S, Berube NG, Dick FA. 2010. Mitotic chromosome condensation mediated by the retinoblastoma protein is tumor-suppressive. *Genes Dev* 24:1351–1363. <https://doi.org/10.1101/gad.1917610>.
- D'Ambrosio C, Schmidt CK, Katou Y, Kelly G, Itoh T, Shirahige K, Uhlmann F. 2008. Identification of cis-acting sites for condensin loading onto budding yeast chromosomes. *Genes Dev* 22:2215–2227. <https://doi.org/10.1101/gad.1675708>.
- Dennis G, Jr, Sherman BT, Hosack DA, Yang J, Gao W, Lane HC, Lempicki RA. 2003. DAVID: database for Annotation, Visualization, and Integrated Discovery. *Genome Biol* 4:P3. <https://doi.org/10.1186/gb-2003-4-9-r60>.
- Wang S, Sun H, Ma J, Zang C, Wang C, Wang J, Tang Q, Meyer CA, Zhang Y, Liu XS. 2013. Target analysis by integration of transcriptome and ChIP-seq data with BETA. *Nat Protoc* 8:2502–2515. <https://doi.org/10.1038/nprot.2013.150>.
- Cecchini MJ, Thwaites M, Talluri S, Macdonald JI, Passos DT, Chong JL, Cantalupo P, Stafford P, Saenz-Robles MT, Francis SM, Pipas JM, Leone G, Welch I, Dick FA. 2014. A retinoblastoma allele that is mutated at its common E2F interaction site inhibits cell proliferation in gene targeted mice. *Mol Cell Biol* 34:2029–2045. <https://doi.org/10.1128/MCB.01589-13>.
- Barski A, Cuddapah S, Cui K, Roh TY, Schones DE, Wang Z, Wei G, Chepelev I, Zhao K. 2007. High-resolution profiling of histone methylations in the human genome. *Cell* 129:823–837. <https://doi.org/10.1016/j.cell.2007.05.009>.
- Wang Z, Zang C, Rosenfeld JA, Schones DE, Barski A, Cuddapah S, Cui K,

- Roh TY, Peng W, Zhang MQ, Zhao K. 2008. Combinatorial patterns of histone acetylations and methylations in the human genome. *Nat Genet* 40:897–903. <https://doi.org/10.1038/ng.154>.
35. Creighton MP, Cheng AW, Welstead GG, Kooistra T, Carey BW, Steine EJ, Hanna J, Lodato MA, Frampton GM, Sharp PA, Boyer LA, Young RA, Jaenisch R. 2010. Histone H3K27ac separates active from poised enhancers and predicts developmental state. *Proc Natl Acad Sci U S A* 107: 21931–21936. <https://doi.org/10.1073/pnas.1016071107>.
 36. Narita M, Nunez S, Heard E, Narita M, Lin AW, Hearn SA, Spector DL, Hannon GJ, Lowe SW. 2003. Rb-mediated heterochromatin formation and silencing of E2F target genes during cellular senescence. *Cell* 113: 703–716. [https://doi.org/10.1016/s0092-8674\(03\)00401-x](https://doi.org/10.1016/s0092-8674(03)00401-x).
 37. Blais A, van Oevelen CJ, Margueron R, Acosta-Alvear D, Dynlacht BD. 2007. Retinoblastoma tumor suppressor protein-dependent methylation of histone H3 lysine 27 is associated with irreversible cell cycle exit. *J Cell Biol* 179:1399–1412. <https://doi.org/10.1083/jcb.200705051>.
 38. Nishide K, Hirano T. 2014. Overlapping and non-overlapping functions of condensins I and II in neural stem cell divisions. *PLoS Genet* 10: e1004847. <https://doi.org/10.1371/journal.pgen.1004847>.
 39. Hocquet C, Robellet X, Modolo L, Sun XM, Burny C, Cuylen-Haering S, Toselli E, Claudier-Munster S, Steinmetz L, Haering CH, Marguerat S, Bernard P. 2018. Condensin controls cellular RNA levels through the accurate segregation of chromosomes instead of directly regulating transcription. *Elife* 7:e38517. <https://doi.org/10.7554/eLife.38517>.
 40. Cai M, Gao F, Lu W, Wang K. 2016. w4CSeq: software and web application to analyze 4C-seq data. *Bioinformatics* 32:3333–3335. <https://doi.org/10.1093/bioinformatics/btw408>.
 41. Sridharan R, Tchiew J, Mason MJ, Yachechko R, Kuoy E, Horvath S, Zhou Q, Plath K. 2009. Role of the murine reprogramming factors in the induction of pluripotency. *Cell* 136:364–377. <https://doi.org/10.1016/j.cell.2009.01.001>.
 42. Liu W, Tanasa B, Tyurina OV, Zhou TY, Gassmann R, Liu WT, Ohgi KA, Benner C, Garcia-Bassets I, Aggarwal AK, Desai A, Dorrestein PC, Glass CK, Rosenfeld MG. 2010. PHF8 mediates histone H4 lysine 20 demethylation events involved in cell cycle progression. *Nature* 466:508–512. <https://doi.org/10.1038/nature09272>.
 43. Longworth MS, Herr A, Ji JY, Dyson NJ. 2008. RBF1 promotes chromatin condensation through a conserved interaction with the Condensin II protein dCAP-D3. *Genes Dev* 22:1011–1024. <https://doi.org/10.1101/gad.1631508>.
 44. Chu WM, Wang Z, Roeder RG, Schmid CW. 1997. RNA polymerase III transcription repressed by Rb through its interactions with TFIIB and TFIIC2. *J Biol Chem* 272:14755–14761. <https://doi.org/10.1074/jbc.272.23.14755>.
 45. Deutschmann E, Longworth MS. 2017. New insights into the pRB/Condensin II interaction. *Cell Cycle* 16:1859–1860. <https://doi.org/10.1080/15384101.2017.1360658>.
 46. Denholtz M, Bonora G, Chronis C, Splinter E, de Laat W, Ernst J, Pellegrini M, Plath K. 2013. Long-range chromatin contacts in embryonic stem cells reveal a role for pluripotency factors and polycomb proteins in genome organization. *Cell Stem Cell* 13:602–616. <https://doi.org/10.1016/j.stem.2013.08.013>.
 47. Imakaev M, Fudenberg G, McCord RP, Naumova N, Goloborodko A, Lajoie BR, Dekker J, Mirny LA. 2012. Iterative correction of Hi-C data reveals hallmarks of chromosome organization. *Nat Methods* 9:999–1003. <https://doi.org/10.1038/nmeth.2148>.
 48. Robinson DR, Wu Y-M, Lonigro RJ, Vats P, Cobain E, Everett J, Cao X, Rabban E, Kumar-Sinha C, Raymond V, Schuetz S, Alva A, Siddiqui J, Chugh R, Worden F, Zalupski MM, Innis J, Mody RJ, Tomlins SA, Lucas D, Baker LH, Ramnath N, Schott AF, Hayes DF, Vijai J, Offit K, Stoffel EM, Roberts JS, Smith DC, Kunju LP, Talpaz M, Cieslik M, Chinnaiyan AM. 2017. Integrative clinical genomics of metastatic cancer. *Nature* 548:297–303. <https://doi.org/10.1038/nature23306>.
 49. Dick FA, Goodrich DW, Sage J, Dyson NJ. 2018. Non-canonical functions of the RB protein in cancer. *Nat Rev Cancer* 18:442–451. <https://doi.org/10.1038/s41568-018-0008-5>.
 50. Manning AL, Dyson NJ. 2012. RB: mitotic implications of a tumour suppressor. *Nat Rev Cancer* 12:220–226. <https://doi.org/10.1038/nrc3216>.
 51. Thwaites MJ, Coschi CH, Isaac CE, Dick FA. 2016. Cell synchronization of mouse embryonic fibroblasts. *Methods Mol Biol* 1342:91–99. https://doi.org/10.1007/978-1-4939-2957-3_5.
 52. Shen Y, Yue F, McCleary DF, Ye Z, Edsall L, Kuan S, Wagner U, Dixon J, Lee L, Lobanenkov VV, Ren B. 2012. A map of the cis-regulatory sequences in the mouse genome. *Nature* 488:116–120. <https://doi.org/10.1038/nature11243>.
 53. Ishak CA, Marshall AE, Passos DT, White CR, Kim SJ, Cecchini MJ, Ferwati S, MacDonald WA, Howlett CJ, Welch ID, Rubin SM, Mann MR, Dick FA. 2016. An RB-EZH2 complex mediates silencing of repetitive DNA sequences. *Mol Cell* 64:1074–1087. <https://doi.org/10.1016/j.molcel.2016.10.021>.
 54. Pedersen MT, Agger K, Laugesen A, Johansen JV, Cloos PA, Christensen J, Helin K. 2014. The demethylase JMJD2C localizes to H3K4me3-positive transcription start sites and is dispensable for embryonic development. *Mol Cell Biol* 34:1031–1045. <https://doi.org/10.1128/MCB.00864-13>.
 55. Langmead B, Salzberg SL. 2012. Fast gapped-read alignment with Bowtie 2. *Nat Methods* 9:357–359. <https://doi.org/10.1038/nmeth.1923>.
 56. Bulut-Karslioglu A, De La Rosa-Velázquez IA, Ramirez F, Barenboim M, Onishi-Seebacher M, Arand J, Galán C, Winter GE, Engist B, Gerle B, O'Sullivan RJ, Martens JHA, Walter J, Manke T, Lachner M, Jenuwein T. 2014. Suv39h-dependent H3K9me3 marks intact retrotransposons and silences LINE elements in mouse embryonic stem cells. *Mol Cell* 55: 277–290. <https://doi.org/10.1016/j.molcel.2014.05.029>.
 57. Thorvaldsdottir H, Robinson JT, Mesirov JP. 2013. Integrative Genomics Viewer (IGV): high-performance genomics data visualization and exploration. *Brief Bioinform* 14:178–192. <https://doi.org/10.1093/bib/bbs017>.
 58. Robinson JT, Thorvaldsdottir H, Winckler W, Guttman M, Lander ES, Getz G, Mesirov JP. 2011. Integrative genomics viewer. *Nat Biotechnol* 29: 24–26. <https://doi.org/10.1038/nbt.1754>.
 59. Quinlan AR, Hall IM. 2010. BEDTools: a flexible suite of utilities for comparing genomic features. *Bioinformatics* 26:841–842. <https://doi.org/10.1093/bioinformatics/btq033>.
 60. Quinlan AR. 2014. BEDTools: the Swiss-Army tool for genome feature analysis. *Curr Protoc Bioinformatics* 47:11.12.1–11.12.34. <https://doi.org/10.1002/0471250953.bi1112s47>.
 61. Ramirez F, Dundar F, Diehl S, Gruning BA, Manke T. 2014. deepTools: a flexible platform for exploring deep-sequencing data. *Nucleic Acids Res* 42:W187–91. <https://doi.org/10.1093/nar/gku365>.
 62. Ramirez F, Ryan DP, Gruning B, Bhardwaj V, Kilpert F, Richter AS, Heyne S, Dundar F, Manke T. 2016. deepTools2: a next generation web server for deep-sequencing data analysis. *Nucleic Acids Res* 44:W160–W165. <https://doi.org/10.1093/nar/gkw257>.
 63. Dobin A, Davis CA, Schlesinger F, Drenkow J, Zaleski C, Jha S, Batut P, Chaisson M, Gingeras TR. 2013. STAR: ultrafast universal RNA-seq aligner. *Bioinformatics* 29:15–21. <https://doi.org/10.1093/bioinformatics/bts635>.
 64. Mouse Genome Sequencing Consortium, Waterston RH, Lindblad-Toh K, Birney E, Rogers J, Abril JF, Agarwal P, Agarwala R, Ainscough R, Alexandersson M, An P, Antonarakis SE, Attwood J, Baertsch R, Bailey J, Barlow K, Beck S, Berry E, Birren B, Bloom T, Bork P, Botcherby M, Bray N, Brent MR, Brown DG, Brown SD, Bult C, Burton J, Butler J, Campbell RD, Carninci P, Cawley S, Chiaromonte F, Chinwalla AT, Church DM, Clamp M, Clee C, Collins FS, Cook LL, Copley RR, Coulson A, Couronne O, Cuff J, Curwen V, Cutts T, Daly M, David R, Davies J, Delehaunty KD, Deri J, et al. 2002. Initial sequencing and comparative analysis of the mouse genome. *Nature* 420:520–562.
 65. Pertea M, Pertea GM, Antonescu CM, Chang TC, Mendell JT, Salzberg SL. 2015. StringTie enables improved reconstruction of a transcriptome from RNA-seq reads. *Nat Biotechnol* 33:290–295. <https://doi.org/10.1038/nbt.3122>.
 66. Pavlidis P, Noble WS. 2003. Matrix2png: a utility for visualizing matrix data. *Bioinformatics* 19:295–296. <https://doi.org/10.1093/bioinformatics/19.2.295>.
 67. Cecchini MJ, Amiri M, Dick FA. 2012. Analysis of cell cycle position in mammalian cells. *JoVE* 59:e3491. <https://doi.org/10.3791/3491>.
 68. Hagège H, Klous P, Braem C, Splinter E, Dekker J, Cathala G, de Laat W, Forné T. 2007. Quantitative analysis of chromosome conformation capture assays (3C-qPCR). *Nat Protoc* 2:1722–1733. <https://doi.org/10.1038/nprot.2007.243>.
 69. Splinter E, Heath H, Kooren J, Palstra RJ, Klous P, Grosveld F, Galjart N, de Laat W. 2006. CTCF mediates long-range chromatin looping and local histone modification in the beta-globin locus. *Genes Dev* 20:2349–2354. <https://doi.org/10.1101/gad.399506>.
 70. Splinter E, de Wit E, van de Werken HJ, Klous P, de Laat W. 2012. Determining long-range chromatin interactions for selected genomic sites using 4C-seq technology: from fixation to computation. *Methods* 58:221–230. <https://doi.org/10.1016/j.ymeth.2012.04.009>.